

Bad metal and negative compressibility transitions in a two-band Hubbard model

Raymond Frésard,^{1,*} Kevin Steffen,² and Thilo Kopp²

¹*Normandie Université, ENSICAEN, UNICAEN, CNRS, CRISMAT, 14050 Caen, France*

²*Center for Electronic Correlations and Magnetism, EP VI,
Institute of Physics, University of Augsburg, 86135 Augsburg, Germany*

(Dated: April 11, 2022)

We analyze the paramagnetic state of a two-band Hubbard model with finite Hund's coupling close to integer filling at $n = 2$ in two spatial dimensions. Previously, a Mott metal-insulator transition was established at $n = 2$ with a coexistence region of a metallic and a bad metal state in the vicinity of that integer filling. The coexistence region ends at a critical point beyond which a charge instability persists. Here we investigate the transition into negative electronic compressibility states for an extended filling range close to $n = 2$ within a slave boson setup. We analyze the separate contributions from the (fermionic) quasiparticles and the (bosonic) multiparticle incoherent background and find that the total compressibility depends on a subtle interplay between the quasiparticle excitations and collective fields. Implementing a Blume-Emery-Griffiths model approach for the slave bosons, which mimics the bosonic fields by Ising-like pseudospins, we suggest a feedback mechanism between these fields and the fermionic degrees of freedom. We argue that the negative compressibility can be sustained for heterostructures of such strongly correlated planes and results in a large capacitance of these structures. The strong density dependence of these capacitances allows to tune them through small electronic density variations. Moreover, by resistive switching from a Mott insulating state to a metallic state through short electric pulses, transitions between fairly different capacitances are within reach.

I. INTRODUCTION.

Strongly correlated electron systems have been in the focus of research for many decades, not the least on account of their peculiar magnetic [1] and unconventional superconducting properties [2–5]. The manifest characteristic of the prominent model for strongly correlated electrons, the one-band Hubbard model [6, 7], is the doping-driven Mott metal-insulator transition (MIT) [8]. It is the repulsive on-site Coulomb interaction U that renders a transition into a Mott insulating state at half-filling ($n = 1$). With respect to MITs, an extension of the model to a multiband case [9–12] appears to be qualitatively similar except that insulating states are to be identified at integer filling numbers. For example, in the case of two orbitals per site insulating states can emerge at $n = 1, 2, 3$ —apart from the uncorrelated insulating states at $n = 0$ and 4.

However, an unsophisticated reasoning with respect to multi-band behavior must fail on several accounts: For asymmetric two-orbital Hubbard models, presenting systems with unequal local Coulomb interactions for distinct orbitals or different band widths, orbital selective Mott phases are to be expected where one band may be insulating whereas the second band is metallic (see, for example, Refs. [13–17]). Moreover, when further coupling parameters become relevant, such as Hund's coupling J_H , various magnetic phases are stabilized [18–21]. Recently, an in-gap band for the two-orbital case [22] has been identified, the width of which depends on J_H [23]. Furthermore, even for modest Coulomb interaction U , Hund's

coupling J_H may strongly reduce the coherence of the underlying uncorrelated metal. This prominently applies to the degenerate three-band Hubbard model around one charge away from half-filling, in the so-called Hund metal regime [24–26].

Intriguing is also the nature of electronic phases in the vicinity of the insulating states at these critical filling factors. If U is on the order of its critical value or above, the electronic state is a bad metal state with correlation-suppressed band width. For a two-band Hubbard model with finite J_H , a first order transition was established from a moderately correlated metallic state into a bad metal, where the transition and the coexistence regime strongly depend on J_H/U and end at a critical point [27]. In particular, the quasiparticle weight $z^2(n)$ collapses to a small value at this transition and, close to $n = 2$, a finite Hund's coupling controls this behavior in the two-orbital case, as correlations then depend on the local spin alignment.

In our work we focus on the transitions into the bad metal behavior and into a negative compressibility state in the vicinity of $n = 2$ for a symmetric two-band Hubbard model with finite coupling J_H . Beyond the first order transition into the bad metal regime [27], a continuous transition—at which the electronic compressibility diverges indicating a charge instability—was previously identified [28]. A different scenario for a strongly enhanced or negative compressibility in a multiband model was suggested for the insulator-metal transition in Sr-doped LaTiO_3 [29]. There, an interorbital charge transfer may result in a negative subband compressibility, assuming that at least one band is close to a Mott transition.

Transitions into a state of negative electronic compressibility were observed experimentally at interface

* Raymond.Fresard@ensicaen.fr

electron gases in Si-MOSFETs and in III-V heterostructures [30–32]. Moreover, electron liquids formed at $\text{LaAlO}_3\text{-SrTiO}_3$ interfaces through electronic reconstruction may allow for negative compressibility [33, 34] as confirmed in Kelvin probe microscopy measurements [34].

It should be noted that a negative electronic compressibility does not necessarily imply a thermodynamic instability—with a possible transition into a phase separated state: the negative (inverse) compressibility may be compensated by positive terms which are generically given by the ionic background or by coupling to further electronic systems, as realized in some heterostructures. Here we do not investigate the nature of the negative compressibility state. It depends on the material and the interplay between local and long range Coulomb interaction. Usually it is expected that the electronic system phase separates or a CDW state is formed. However, these may be exponentially damped [35] and the state stays rather homogeneous with a negative compressibility as at $\text{LaAlO}_3\text{-SrTiO}_3$ interfaces.

Not surprisingly, in a one-band Hubbard model the compressibility of the paramagnetic state is reduced with respect to its free electron value and stays positive, yet strikingly the compressibility is a non-monotonous function of U for electron densities in proximity to half-filling. The reduction is controlled by the interplay of the effective mass and the Landau parameter F_0^s [36–38]. The same is true in the vicinity of the MITs at $n = 1, 3$ in the two-band Hubbard model but the case of $n = 2$ is fascinatingly different. There, a finite J_H aligns the spins in the two different orbitals of a site which induces a suppression of orbital fluctuations in the vicinity of $n = 2$ [27, 28]. Nevertheless, it is remarkable that a repulsive local Coulomb interaction induces a negative compressibility state.

Here, we analyze the interplay of quasiparticle behavior, expressed by the quasiparticle weight $z^2(n)$, and collective excitations, expressed by bosonic fields for orbital occupations in the two-band Hubbard model. The feedback between these fermionic and bosonic degrees of freedom determines the discontinuous and continuous phase transitions and drives the electronic system into a state of negative compressibility.

The slave boson technique is well adjusted to study this interplay. In fact, negative electronic compressibility obtained by means of Kotliar-Ruckenstein and related slave boson calculations received considerable attention in the context of the Hubbard model on the square lattice. In the course of considering incommensurate spiral phases—which allow to lower the energy of the lightly doped one-band Hubbard model with respect to the commensurate antiferromagnetic phase—negative compressibility in a small density range close to half band filling was discovered [39]. Motivated by the quest of thermodynamically stable phases a Maxwell construction was suggested, which has been recently revisited [40].

A well accessible response function to probe the com-

pressibility is the capacitance of heterostructures comprising two electrodes and dielectric layers in between. An enhancement of the capacitance in two-band systems was suggested in Ref. [41]. Besides, the capacitance of multilayers with strongly correlated materials was investigated recently [38, 42, 43], either with a barrier or electrodes consisting of strongly correlated materials. The capacitance strongly depends on the correlation strength U of the considered one-band models. In the present work we suggest a realization of a capacitance device which comprises plates with a material that is electronically in a regime well described by a two-band Hubbard model close to half filling.

The paper is organized as follows: the two-band Hubbard model of our investigation is presented in Sec. II, together with the key features of the extended Kotliar-Ruckenstein slave-boson technique that we utilize. We present our results in Sec. III. These comprise the quasiparticle residue z^2 and the phase diagram close to half filling in Sec. III A, then the double occupancies as represented by slave boson fields in Sec. III B, the electronic compressibility κ in Sec. III C, and eventually the capacitance of a device with strongly correlated electron systems on the electrodes in Sec. III D. In Sec. IV the bosonic degrees of freedom are interpreted in terms of classical Ising-fields through a Blume-Emery-Griffiths (BEG) model approach, and a feedback mechanism between these fields and the fermionic degrees of freedom is presented. Finally, Sec. V concludes the paper with summary and outlook.

The gauge symmetry group of the approach is unraveled in Appendix A, while the saddle point equations that we solve are detailed in Appendix B. The filling dependence of the chemical potential is given in Appendix C and the single and triple occupancies are addressed in Appendix D. The parameters that enter the BEG-type analysis are discussed in Appendix E, and the BEG phase diagram for the chosen set of parameters in Appendix F.

II. MODEL AND METHOD

The microscopical model consists of a kinetic energy term \hat{H}_0 and a Hubbard interaction part \hat{H}_i , with the complete Hamiltonian $\hat{H} = \hat{H}_0 + \hat{H}_i$. The kinetic term reads for the two-band case

$$\hat{H}_0 = \sum_{\mathbf{k}, \sigma} \begin{pmatrix} c_{\mathbf{k}, \eta, \sigma}^\dagger & c_{\mathbf{k}, \xi, \sigma}^\dagger \end{pmatrix} \begin{pmatrix} \varepsilon_{\eta, \mathbf{k}} & r_{\mathbf{k}} \\ r_{\mathbf{k}} & \varepsilon_{\xi, \mathbf{k}} \end{pmatrix} \begin{pmatrix} c_{\mathbf{k}, \eta, \sigma} \\ c_{\mathbf{k}, \xi, \sigma} \end{pmatrix}. \quad (1)$$

A specific realization one may wish to consider is provided by oxides with two bands active at the Fermi energy. Below, we focus on two degenerate d_{xz} and d_{yz} orbitals dispersing on a square lattice in the x - y plane—with lattice constant a . In that case, a minimal tight-binding model entails $\varepsilon_{\eta/\xi, \mathbf{k}} = -2t \cos(k_x/y a)$ with minimal mixing $r_{\mathbf{k}} = -4t' \sin(k_x a) \sin(k_y a)$. The operators $c_{\mathbf{k}, \eta, \sigma}^\dagger$ ($c_{\mathbf{k}, \xi, \sigma}^\dagger$) create a Bloch eigenstate with wave vector

\mathbf{k} and spin projection σ in band η (ξ). Below we refer to a band index u that takes the values η, ξ . As t' is expected to be much smaller than t we use the representative value $t'/t = 1/25$ in our numerical evaluations. In this case the bandwidth W is given by $W = 4t$, and we will use from now on W as the band parameter instead of t .

The two non-interacting bands $\epsilon_{\mathbf{k},\nu}^{(0)}$ follow as

$$\epsilon_{\mathbf{k},\nu}^{(0)} = \frac{1}{2} \left(\varepsilon_{\eta,\mathbf{k}} + \varepsilon_{\xi,\mathbf{k}} + \nu \sqrt{(\varepsilon_{\eta,\mathbf{k}} - \varepsilon_{\xi,\mathbf{k}})^2 + 4r_{\mathbf{k}}^2} \right) \quad (2)$$

with $\nu = \pm 1$. While these bands produce a van Hove singularity at the bottom and the top of the bands, akin to one-dimensional systems, their dispersion is truly two-dimensional. Our results do not depend qualitatively on this choice but rather on the relative magnitudes of the band width, Hund's coupling J_H and on-site Coulomb interaction $U_{P/A/H}$ (see below).

For the local part of the Hamiltonian,

$$\begin{aligned} \hat{H}_i = & U_P \sum_{i,\sigma} \hat{n}_{i,\eta,\sigma} \hat{n}_{i,\xi,\sigma} + U_A \sum_{i,\sigma} \hat{n}_{i,\eta,\sigma} \hat{n}_{i,\xi,-\sigma} \\ & + U_H \sum_{i,u=\eta,\xi} \hat{n}_{i,u,\uparrow} \hat{n}_{i,u,\downarrow} \end{aligned} \quad (3)$$

the interactions of the electrons between different bands are taken into account: The first term originates from the interaction of electrons in different orbitals with parallel spins and the second term from the interaction between electrons in different orbitals with antiparallel spins. The last term, which also appears in the single-band Hubbard model, is due to the on-site repulsion between two electrons in the same band. Above, $\hat{n}_{i,u,\sigma} = c_{i,u,\sigma}^\dagger c_{i,u,\sigma}$ is the number operator on site i , in band u and spin projection σ . For an ion in the octahedral environment, assumed here, the coefficients of the interaction are related by $U_A = U_P + J_H$ and $U_H = U_P + 3J_H$ [11, 44, 45]. As argued in Ref. [28] further contributions from Hund's coupling are of minor relevance for the considered regime. They are not considered in this work.

We use an extended Kotliar-Ruckenstein slave-boson technique [46] to treat the above defined two-band Hamiltonian. One slave-boson field is introduced for each of the sixteen possible atomic configurations [11], as well as four fermionic fields $f_{i,\alpha}$. The physical electron annihilation operators may be expressed in terms of auxiliary particles as:

$$c_{i,\alpha} = z_{i,\alpha} f_{i,\alpha}, \quad (4)$$

where $\alpha = (u, \sigma)$ is a four-valued spin-band index and $z_{i,\alpha}$ is a combination of bosonic operators as given in Ref. [11] (see also Appendix A). A bosonic field e (ϖ) is associated to empty (fourfold occupied) sites, and four bosonic fields p_α (t_α) are associated to each singly (triply) occupied sites whereby the α -state is filled (empty). The six different double occupancies are tied to bosons $d_{\alpha,\alpha'}$, with $\alpha < \alpha'$. All auxiliary fermionic and bosonic fields satisfy

canonical commutation relations, while the physical electron operators do so provided the following constraints are satisfied:

$$\begin{aligned} 1 = & e_i^\dagger e_i + \sum_{\alpha} p_{i,\alpha}^\dagger p_{i,\alpha} + \sum_{\alpha < \alpha'} d_{i,\alpha\alpha'}^\dagger d_{i,\alpha\alpha'} \\ & + \sum_{\alpha} t_{i,\alpha}^\dagger t_{i,\alpha} + \varpi_i^\dagger \varpi_i \end{aligned} \quad (5)$$

$$\begin{aligned} f_{i,\alpha}^\dagger f_{i,\alpha} = & p_{i,\alpha}^\dagger p_{i,\alpha} + \sum_{\alpha' < \alpha} d_{i,\alpha\alpha'}^\dagger d_{i,\alpha\alpha'} + \sum_{\alpha' > \alpha} d_{i,\alpha\alpha'}^\dagger d_{i,\alpha\alpha'} \\ & + \sum_{\alpha' \neq \alpha} t_{i,\alpha'}^\dagger t_{i,\alpha'} + \varpi_i^\dagger \varpi_i \end{aligned} \quad (6)$$

In an imaginary time functional integral the constraints (5) and (6) are incorporated in the Lagrangian together with the (Lagrange multiplier) constraint fields λ' and λ_α , respectively. Ideally the functional integrals should be calculated exactly. Regarding spin models this has been achieved for the Ising chain [47], but in the case of interacting electron models exact evaluations could be performed on small clusters only, either using the Barnes representation [48], or the Kotliar and Ruckenstein representation [49]. Yet, such a calculation remains challenging on lattices of higher dimensionality, and we rather resort to the saddle-point approximation.

Below, we consider the paramagnetic saddle-point approximation obtained after having integrated out the fermionic fields (for formal aspects of the approach see Appendix B). In the paramagnetic phase one may introduce d_P^2 , d_A^2 , and d_H^2 , through the relations $d_{\eta\uparrow,\xi\uparrow}^2 = d_{\eta\downarrow,\xi\downarrow}^2 \equiv d_P^2$, $d_{\eta\uparrow,\xi\downarrow}^2 = d_{\eta\downarrow,\xi\uparrow}^2 \equiv d_A^2$, $d_{\eta\uparrow,\eta\downarrow}^2 = d_{\xi\uparrow,\xi\downarrow}^2 \equiv d_H^2$, as well as p^2 , t^2 , and λ through $p^2 \equiv p_\alpha^2$, $t^2 \equiv t_\alpha^2$, and $\lambda \equiv \lambda_\alpha \forall \alpha$. In terms of them, the grand potential may be written as:

$$\begin{aligned} \Omega/N_L = & 2 (U_P d_P^2 + U_A d_A^2 + U_H d_H^2) \\ & + 2 (U_P + U_A + U_H) (2t^2 + \varpi^2) \\ & + \lambda' (e^2 + 4p^2 + 2(d_P^2 + d_A^2 + d_H^2) + 4t^2 + \varpi^2 - 1) \\ & - 4\lambda (p^2 + d_P^2 + d_A^2 + d_H^2 + 3t^2 + \varpi^2) \\ & - \frac{2}{\beta} \frac{1}{N_L} \sum_{\mathbf{k},\nu} \ln (1 + e^{-\beta E_{\mathbf{k},\nu}}). \end{aligned} \quad (7)$$

In order to disburden the notation we use $U \equiv U_P$ below. Outside the strong coupling regime $U > 5W$ in which the ϖ boson representing the four-fold occupancy was neglected, all bosons were retained in our calculations performed for $n \leq 2$. Results for $n \geq 2$ are obtained using particle-hole symmetry. Here $\beta = 1/k_B T$ incorporates the temperature T and N_L is the number of lattice sites. The dispersion for the quasiparticles is given by

$$E_{\mathbf{k},\nu} = z^2 \epsilon_{\mathbf{k},\nu}^{(0)} - \mu_{\text{eff}} \quad (8a)$$

$$\mu_{\text{eff}} = \mu - \lambda. \quad (8b)$$

For more details about the saddle-point equations see Appendix B.

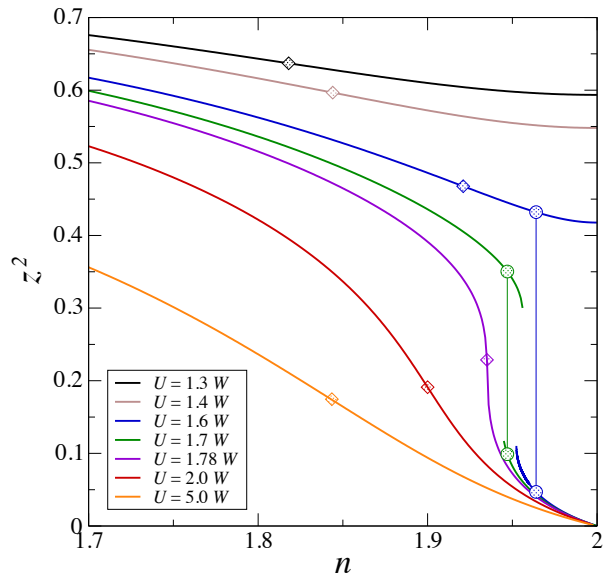


FIG. 1. Quasiparticle residue in dependence on filling n for $J_H = W/6$. The circles and the vertical thin lines characterize the first order transitions while the diamonds mark the inflection points.

III. RESULTS

The transition to a negative compressibility in proximity to half filling is a remarkable feature of the two-band Hubbard model [28], a property which is not found for the one-band Hubbard model. A first order phase transition to a bad metal state close to half-filling was identified before [27]. There the quasiparticle residue of the charge carriers drops significantly to low values, concomitant with a jump of the effective mass to large values. These transitions are controlled by Hund's coupling J_H , that is, they are absent for vanishing J_H . We emphasize that J_H does not scale with U but rather depends on the orbital character of the electrons. For our investigation of the impact of intermediate to strong correlations on the electronic compressibility we consider J_H of the order of t , namely we fix $J_H = W/6$. A J_H/U dependence was discussed in Ref. [27, 28]. The full J_H dependence will be the scope of a different work.

A. Quasiparticle residue and phase diagram

The dependence of the quasiparticle residue z^2 on charge carrier density and interaction strength in the two-band model has been extensively investigated before (see for example Refs. [11, 12, 27, 50]), not the least because it is directly related to the inverse effective electronic mass. Of particular interest is its behavior at the commensurate densities: for $n = 1$ and $n = 3$ it decreases smoothly with increasing interaction strength, and vanishes at the metal-to-insulator transition. It is a continuous transi-

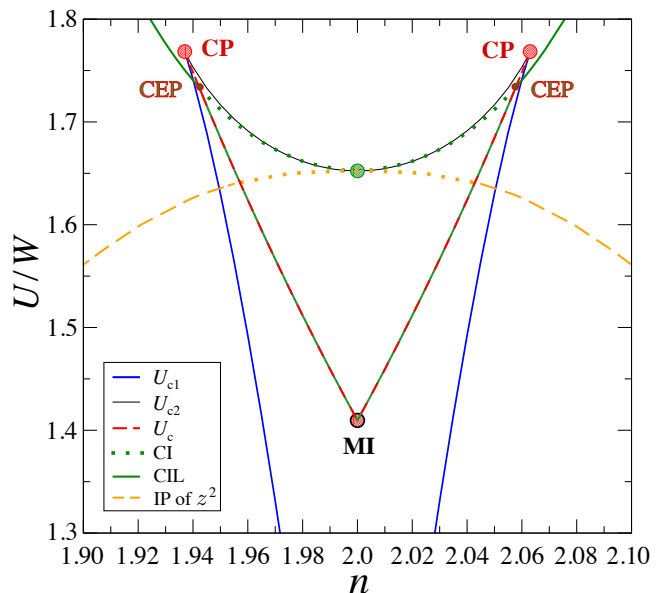


FIG. 2. Phase diagram for $J_H = W/6$. The red dashed line separates a stable metallic solution from a stable bad metal state at larger values of U . This line becomes red-green dashed where the charge instability coincides with that first order transition. U_{c1} and U_{c2} mark the boundary of the coexistence regime. The red circles locate the critical points $CP = (n^*, U_c^*)$ and $(2 - n^*, U_c^*)$. The green circle denotes $(n = 2, U_{c2}(n = 2))$. The charge instability line (CIL) merges with the U_c -line at the critical end point (CEP) marked by the red-green dot (see the magnification of this regime in Fig. 3). The first order transition (red-green dashed line) ends at the MI-transition point, close to $(n = 2, U/W = 1.41)$. The green dots extend the charge instability (CI) into the metastable metallic state. The orange dashed (dotted) curve marks the inflection points of $z^2(n)$ in the metallic (metallic metastable) phase.

tion, and bears much resemblance with the Brinkman-Rice transition [8]. On the contrary, it is first order for $n = 2$ [27].

Here we consider a fixed parameter value $J_H = W/6$ and plot the quasiparticle residue against filling for various values of U (see Fig. 1). Its behavior varies strongly with the correlation strength: for $U < U_{MI} \simeq 1.41 W$ the quasiparticle residue smoothly depends on filling below the Mott insulator transition (MI). As previously shown in Ref. [11], it displays a broad minimum at $n = 2$ and decreases with increasing U .

The same seems to apply for U up to $1.65 W$, but this is a fallacy. Indeed, a second solution starting from $n = 2$ with $z = 0$ develops and is actually stabilized in a doping range around half-filling that grows with increasing U . This marks a coexistence region of the above described metallic state with this insulating-like doped Mott insulator or “bad metal” state. The bad metal state disappears below an n -dependent value $U_{c1}(n)$ and the metallic state above a value $U_{c2}(n)$ (see blue and black

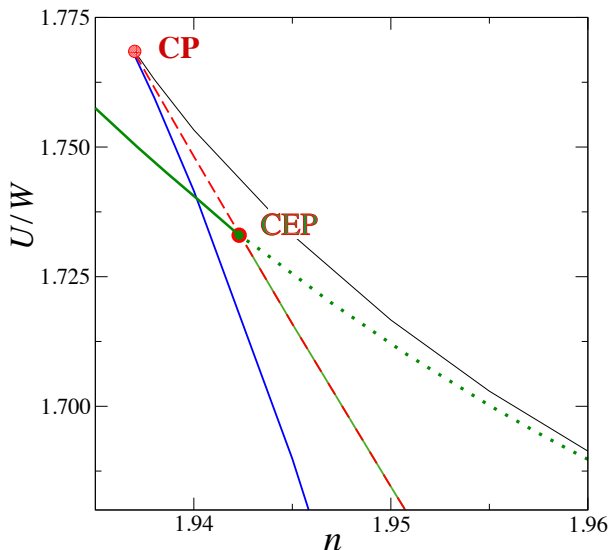


FIG. 3. Phase diagram of Fig. 2 zoomed into filling range close to the critical end point (CEP).

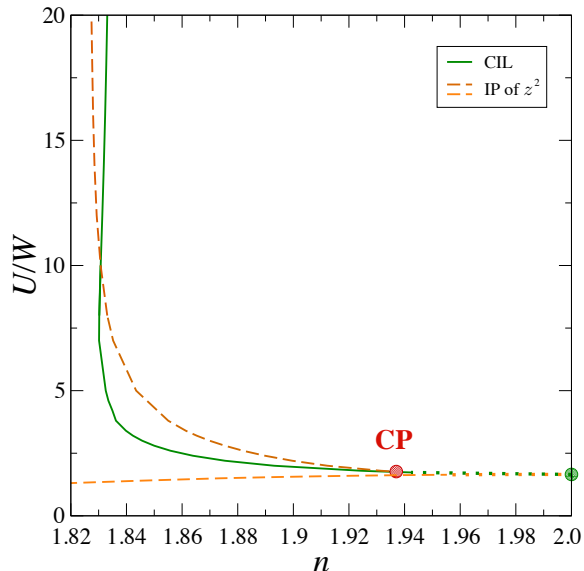


FIG. 4. Charge instability line (CIL) and lines of inflection points of z^2 in the (n, U) phase diagram for $J_H = W/6$. The red circle marks (n^*, U_c^*) , and the green circle ($n = 2, U_{c2}(n = 2)$). The dark-orange dashed line displays the inflection points of $z^2(n)$ for U above U_c^* . The light-orange dashed line denotes the inflection points in the metallic regime (cf. to the diamonds in Fig. 1) and the light-orange dots extend this line of inflection points into the metastable metallic state close to half filling.

curves in Fig. 2, respectively, where the phase diagram is presented, as well as in Figs. 3 and 4.). The lowest value of U_{c2} is $U_{c2}(n = 2) \simeq 1.65 W$ for $J_H = W/6$. The metallic and the insulating-like solutions are degenerate along the red dashed lines in Fig. 2. As a hallmark of this first order transition, the coexistence range of the two solu-

tions is rather limited in size and extends from $U = U_{MI}$ at half-filling to at most $n^* \simeq 1.937$ for $U_c^* \simeq 1.777 W$. Beyond it, both solutions turn indistinguishable and accordingly smoothly connect.

At the critical point CP, located at (n^*, U_c^*) , the residue z^2 possesses an inflection point in its density dependence, where its derivative diverges. When further increasing U , there remains an inflection point, where the magnitude of the slope steadily decreases (see the diamonds placed on the continuous curves in Fig. 1 and the dark-orange dashed line in Fig. 4). As the addressed jump of the quasiparticle residue for $U < U_c^*$ transforms into an inflection point in its density dependence, it is to be associated with a crossover. For $U < U_{MI}$, besides the stable metallic solution, there remains a solution arising from the Mott insulator. It is metastable and, therefore, it will not be addressed any longer in the following.

In addition, we display the charge instability line (CIL) of the metallic solution as continuous green lines in Figs. 2, 3, and 4. Along this line the inverse electronic compressibility is zero. The CIL merges with the U_c -line at $(n_{CEP} \simeq 1.9423, U_{CEP} \simeq 1.733 W)$ (see Fig. 3). Below this value of U , the U_c -line not only represents the transition from metallic to bad-metal behavior but also a discontinuity of κ^{-1} (jump from positive to negative values of κ^{-1}). The analysis of the charge instability will be presented in Sec. III C.

B. Slave boson fields

The slave boson expectation values represent collective fields. With the calculations performed at fixed J_H the collective fields involving double occupancies markedly differ from one another in a broad density range around half-filling. As shown in Fig. 5, the hierarchy $d_H^2 < d_A^2 < d_B^2$ is always clearly obeyed, with the exception of the Mott insulating phase where the first two vanish. The critical point (n^*, U_c^*) illuminates the density dependence of all bosons; there, they all exhibit an inflection point with diverging derivative with respect to n . For $U > U_c^*$ inflection points remain, though the amplitude of the derivatives diminishes. On the other side, $U < U_c^*$, all boson expectation values jump at the first order transition whereas a smooth behavior is restored for $U < U_c(n = 2)$. In reference to the Mott insulator transition we denote this point as (MI).

C. Compressibility

The inverse electronic compressibility is expressed through the derivative of the chemical potential μ with respect to the electronic density ρ

$$\kappa^{-1} = \rho^2 \frac{\partial \mu}{\partial \rho} \quad (9)$$

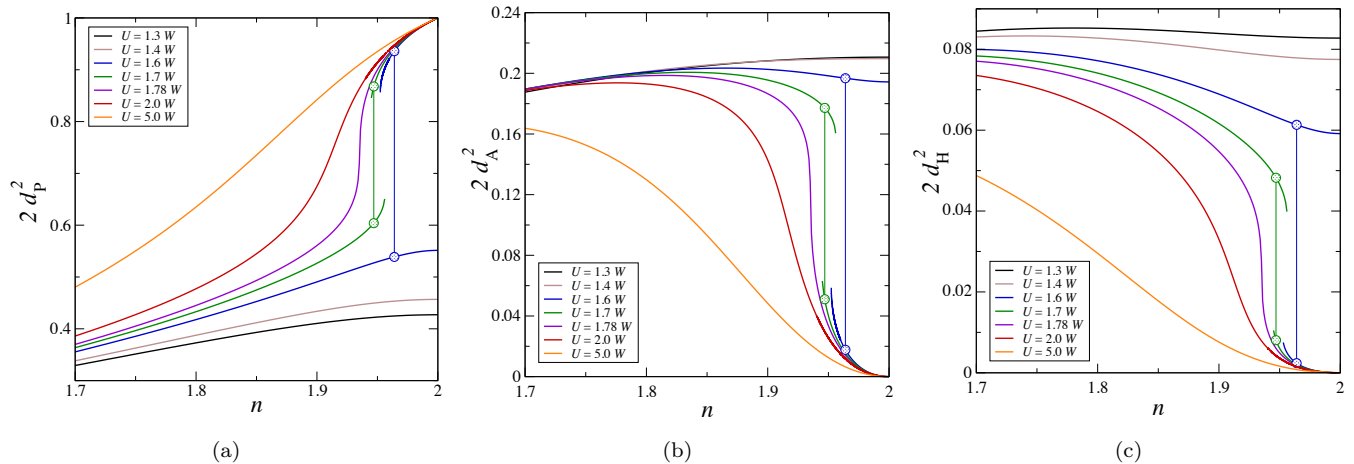


FIG. 5. Filling-dependent expectation values of site double occupancies for $J_H = W/6$: (a) two parallel spins, (b) two anti-parallel spins in different orbitals, (c) two anti-parallel spins in the same orbital. The circles and the vertical thin lines characterize the first order transitions.

where we consider the zero-temperature compressibility for constant volume. The density in the two-dimensional electronic system is trivially related to the filling through $n = a^2\rho$ where a is the lattice constant. Alternatively, the inverse compressibility may be calculated directly from $F(n)$, which is the Legendre transform of $\Omega(\mu)$, through $\kappa^{-1} = n^2 d^2(F/N_L a^2)/d^2 n$.

In this work we ascribe a continuous transition with a zero crossing in the inverse electronic compressibility $\kappa^{-1}(n)$ to a charge instability (see the green lines in Figs. 2 and 4). There the charge susceptibility κ diverges. On the other hand, a first order transition emerges if $\kappa^{-1}(n)$ changes discontinuously and the charge susceptibility stays finite. This discontinuity is tied to the metal to bad metal transition (see the green-red lines in Fig. 2). Only at singular points $(n_{\text{CEP}}, U_{\text{CEP}})$, the inverse compressibility approaches zero from the low-filling side and jumps to a negative value (see the green-red point in Fig. 3). There the charge instability line ends at the first order transition line. In analogy with similar end points in thermodynamic phase transitions we denote this point as a “critical end point” (CEP).

We now analyze the formation of a negative compressibility state in few of the involved fermionic and bosonic degrees of freedom. The grand potential Ω , Eq. (7), as well as F is made of a fermionic contribution arising from the quasi-particles, and a bosonic one, to which no coherence may be related. Accordingly, the full inverse compressibility κ^{-1} consists of a fermionic contribution κ_f^{-1} , arising from the last two lines of Eq. (7), and a bosonic one κ_b^{-1} , deduced from the first three lines of Eq. (7). Note that the last line is the kinetic energy for a fermionic system and the second but last line contains a contribution to the constraint which relates the fermionic to the bosonic degrees of freedom.

The interaction distinctly influences κ_b^{-1} as may be

deduced from Fig. 6(a). For weak to moderate coupling $U \lesssim 1.4 W$ all bosons display a comparatively weak density dependence and this holds true for κ_b^{-1} as well. For U above U_{MI} , the bosonic contribution to κ^{-1} is still positive but jumps to a larger value close to half-filling. Then, for $U > U_{c2}(2)$, the metastable metallic state does not extend to $n = 2$ and κ_b^{-1} is negative in a wide filling regime well below half-filling before it jumps to a positive value close to half-filling. Eventually, for $U \geq U_c^*$, κ_b^{-1} is continuous with a minimum and a maximum below and above the transition, respectively (see inset of Fig. 6(a)).

In order to relate these findings to the bosonic fields one may rewrite the bosonic contribution Ω_b to the grand potential Eq. (7) as

$$\Omega_b/N_L = -d_P^2 (U + 4J_H) - d_A^2 (U + 2J_H) - d_H^2 (U - 2J_H) \quad (10)$$

This expression results from first neglecting the very small contributions from the bosons e and ϖ , and second to using the constraints to express the boson t in terms of the d -bosons. This additionally yields terms proportional to $n - 1$, but the latter do not contribute to the inverse compressibility—as κ^{-1} is the second derivative with respect to n —and they are not included in Ω_b of Eq. (10) for the following discussion of κ_b^{-1} .

Recalling the above hierarchy among the d -bosons it turns out that the leading contribution to Ω_b follows from the d_P -boson. At $U = U_c^*$ the d_P -boson possesses an inflection point in its density dependence that is located at $n = n^*$. It separates a density range where the density dependence of d_P^2 is characterized by a positive curvature from a regime with a negative curvature (compare the purple curve in Fig. 5(a)). This sign change of the curvature persists for larger U values, which is reflected in κ_b^{-1} (see inset of Fig. 6). This is also true for $U < U_c^*$ but close to it—with the additional feature of a jump at the first order phase transition.

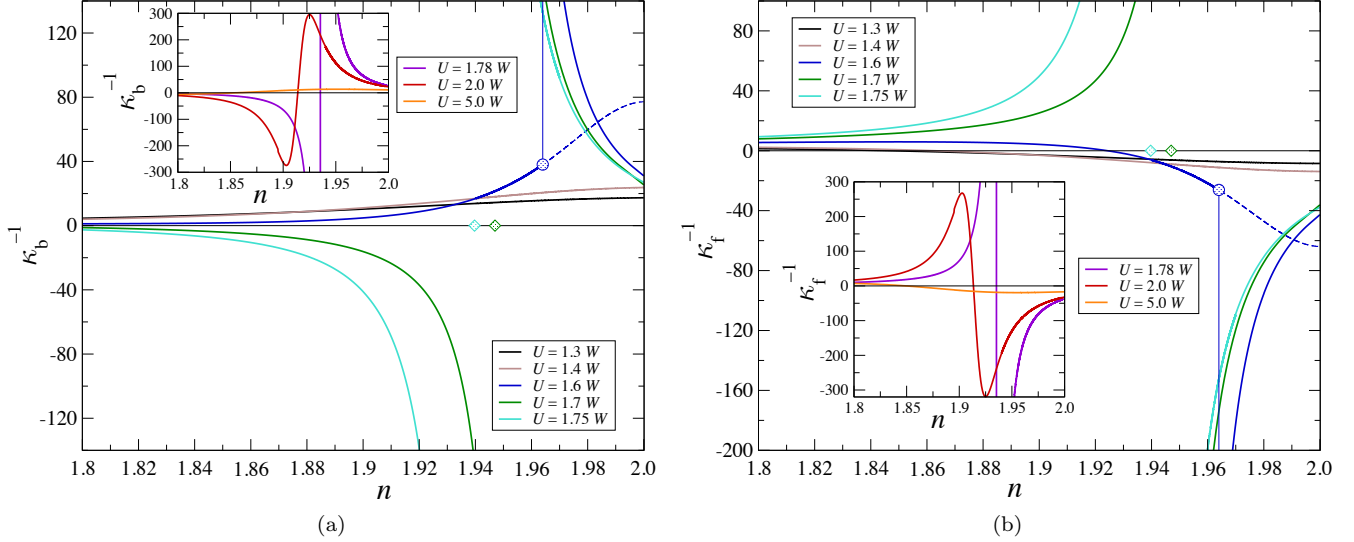


FIG. 6. Bosonic (a) and fermionic (b) contribution to the inverse compressibility in dependence on filling n for $J_H = W/6$. Here $\kappa_{b,f}^{-1}$ is in units of W/a^2 . The vertical blue line marks a first order transition for $U = 1.6 W$. The dashed blue line represents the metastable metallic case. The positions of the first order transitions for $U = 1.7 W$ and $1.75 W$ are schematized by diamonds. The transitions in the inset are continuous albeit the inverse compressibility for $U = 1.78 W$ is not displayed completely.

For weak to moderate coupling $U < U_{MI}$ the curvature of the d_P -boson contribution is negative in the entire presented density range. As this is in fact the leading contribution to κ_b^{-1} , it results necessarily in a positive bosonic compressibility.

For $U \gtrsim U_{MI}$, the density dependence of d_P^2 displays a negative curvature in the considered regime close to half filling. In this case, κ_b^{-1} remains positive. However, well below half-filling the curvature switches its sign as seen for the blue curve in Fig. 5(a) even though the compressibility stays positive. This seeming inconsistency is resolved by the observation that the contribution of the other two d -bosons in Eq. (10) overcompensates the one of d_P for this doping regime far from half filling.

The filling dependence of the fermionic contribution κ_f^{-1} to the inverse compressibility is to a large extent opposite to that of the bosonic κ_b^{-1} (see Fig. 6(b)). Again, the qualitative behavior of such a contribution to the inverse compressibility can be derived from a single dominant term, namely the second derivative of the quasiparticle residue with respect to filling.

In order to understand this we analyze the free energy arising from the grand potential at $T = 0$. The last two lines of Eq. (7)—together with the Legendre transformation—lead to a fermionic contribution F_{kin} to the free energy composed of the kinetic energy, only. Since F_{kin} may be obtained analytically in the limit $t' \rightarrow 0$ with little impact on the numerical results, we adopt this approximation below. In that case we obtain the kinetic energy per site as

$$F_{kin}/N_L = -2z^2 \frac{W}{\pi} \cos\left(\frac{\pi\delta}{4}\right) \quad (11)$$

where doping $\delta \equiv n - 2$ was introduced for convenience. From Eq. (11) one may infer the leading contribution to κ_f^{-1} to be given by

$$\kappa_f^{-1} \simeq -2n^2 \frac{\partial^2 z^2}{\partial n^2} \frac{W}{\pi} \cos\left(\frac{\pi\delta}{4}\right). \quad (12)$$

Numerical tests prove Eq. (12) to be a good approximation.

In the regime of weak to moderate coupling ($U \lesssim U_{MI}$) the effective mass $\sim 1/z^2$ weakly depends on filling, though featuring an inflection point (cf. the position of the diamonds in Fig. 1 and the light-orange dashed line in Fig. 4) at which the curvature switches from negative to positive when increasing the filling. Accordingly, κ_f^{-1} takes comparatively small values, exhibits a sign change, and its magnitude somewhat increases in the vicinity of half filling. When intermediate coupling is considered in the metallic phase ($U \simeq 1.6 W$) the same trends are followed, yet with a larger magnitude and, close to half filling, a jump of the fermionic inverse compressibility to a larger negative value in the stable bad metal state. For larger interaction strength, ($U_{c2}(2) \leq U \leq U_c^*$) the inflection point of z^2 vanishes. Instead, increasingly negative curvature is realized in the entire metallic phase, while positive curvature characterizes the bad metal phase. Note that the corresponding values taken by κ_f^{-1} close to the discontinuity are too large to be displayed in Fig. 6(b). Once U exceeds U_c^* , the inflection point of z^2 is restored, and so is the zero of κ_f^{-1} . Let us stress that it remains a continuous function of density that takes very large positive and negative values (see the purple curve in the inset of Fig. 6(b)).

Since κ_b^{-1} is mainly controlled by the d_p -boson while κ_f^{-1} is primarily ruled by the inverse effective mass, that itself depends on the d_p -boson, one may wonder why these two contributions to κ^{-1} do compete. To that aim we seek for an approximate but reasonably accurate analytical form of $\partial^2 z^2 / \partial n^2$ that enters Eq. (12). From the plethora of contributions to it (cf. Eq. (A4) and the definitions in Eq. (A5)), it turns out that

$$\frac{\partial^2 z^2}{\partial n^2} \simeq \frac{4(d_P + d_A + d_H)^2}{1 - \left(\frac{n-2}{2}\right)^2} \frac{\partial^2(p+t)^2}{\partial n^2} \quad (13)$$

is a good approximation. Here a numerical test shows that the term with the second derivative of d_P^2 is small as compared with the retained term (13) (cf. Figs. 15(a) and (b) to Fig. 5(a)). Hence, while the sign of κ_b^{-1} is essentially given by the curvature of d_P^2 , the one of κ_f^{-1} follows from the curvature of $(p+t)^2$. Fig. 5(a) and Fig. 15(a) and (b) show that they are opposite in sign in the largest part of the parameter space of interest where they therefore compete.

The total inverse compressibility is shown in Fig. 7. The near cancellation of κ_b^{-1} and κ_f^{-1} is particularly clear for the smallest densities. There, not only the magnitude of κ^{-1} is smaller than the larger of its components, but its U -dependence is strongly suppressed. For weak to moderate U ($U \lesssim U_{\text{MI}}$), and under an increase in density, the bosonic contribution takes over in the entire presented density range, where κ^{-1} remains positive.

For intermediate coupling, $U_{\text{MI}} < U < U_c^*$, the sign of κ^{-1} follows mostly the one of κ_f^{-1} . However note that the strong increase of κ_f^{-1} on the low-filling side of the discontinuity is nearly canceled by κ_b^{-1} . Therefore the charge instability (with negative compressibility) is formed already in the stable metallic state (see the turquoise curve in Fig. 7). That regime is identified in the phase diagram of Fig. 2 where for fixed U close to but below U_c^* one first crosses the charge instability line (CIL) with increasing n and only then observes for slightly larger filling a transition to a bad metal state. This regime ends at $(n_{\text{CEP}} \simeq 1.9423, U_{\text{CEP}} \simeq 1.733 W)$ where the CIL merges with the U_c -line (see the red-green point in the inset of Fig. 2).

For U -values above U_c^* the inverse compressibility is continuous—as are its partial contributions κ_f^{-1} and κ_b^{-1} —and the CIL stays at the lower filling side with respect to the line of inflection points (see Fig. 4) for U/W below approximately 10. Again, it is the bosonic contribution which drives the compressibility to negative values before the fermionic contribution beyond the inflection point enforces the negative compressibility state.

D. Capacitance of a heterostructure

Previous studies point out a tendency for the capacitance of heterostructures comprising strongly correlated

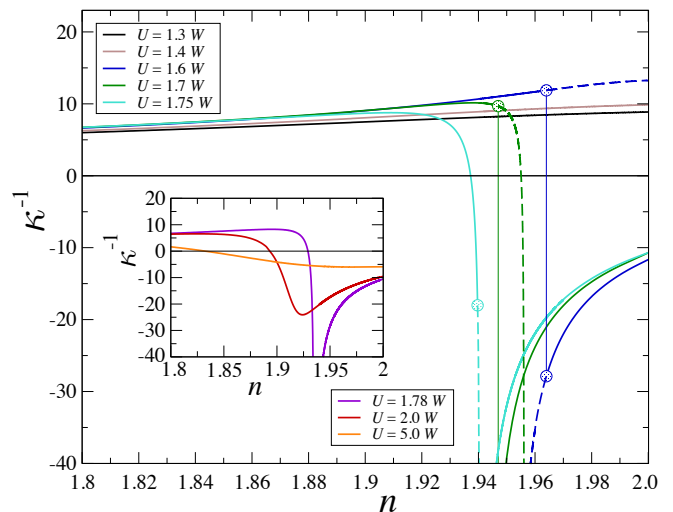


FIG. 7. Inverse compressibility in dependence on filling n for $J_H = W/6$. Here κ^{-1} is in units of W/a^2 . The vertical blue line marks a first order transition for $U = 1.6 W$. The dashed lines refer to the metastable states.

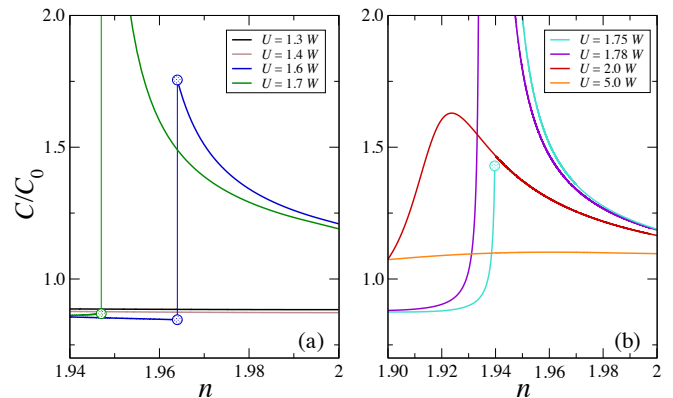


FIG. 8. Capacitance enhancement in dependence on filling n for $J_H = W/6$. (a) The weak coupling regime displays a continuous filling dependence of C/C_0 with values below 1.0 whereas the intermediate coupling range shows jumps of C/C_0 from less than 1 to values well beyond 1. The jumps of the capacitance are associated to the first order metal to bad metal transition and are indicated by vertical lines. (b) For stronger coupling in the range from U_{CEP} to U above U_c^* , the C/C_0 -lines have two branches with a negative capacitance in between. For large coupling beyond U_c^* , the filling dependence of C/C_0 is again continuous.

electron systems to be larger than those with weakly interacting electron systems [38, 51]. Here, we consider a capacitor made of a polarizable dielectric between two electrodes as modeled by the current two-band Hubbard model. In this simple set-up, the quantum corrections to the inverse capacitance (see, e.g. Ref. [41]) are given by

$$\frac{C_0}{C} = 1 + 2 \frac{\varepsilon_0 \varepsilon a^2}{e^2 d} \frac{\partial \mu}{\partial n}. \quad (14)$$

Here, $C_0 = \varepsilon_0 \varepsilon A/d$ is the geometric capacitance of a capacitor with two plates, ε is the dielectric constant of the dielectric material between the two electrodes, each of area A , and d is the thickness of the dielectric. To be specific, we use the parameter values $d/\varepsilon = 4a_B$ (with a_B the Bohr radius), and the lattice spacing a is set to $6a_B$. The prefactor of $\partial\mu/\partial n$ in Eq. (14) is then $2\varepsilon_0 \varepsilon a^2/(e^2 d) = 0.0526 \text{ eV}^{-1}$.

As can be seen in Fig. 14 the chemical potential steadily grows with density in the largest part of the phase diagram. This includes the weak coupling regime $U \leq U_{\text{MI}}$ for all densities as well as the moderate to strong coupling regime for large doping. In these regimes the kinetic term rather acts to lower the capacitance.

For moderate coupling in the range from $U \simeq U_{\text{MI}}$ to $U \lesssim U_{\text{CEP}}$ the metallic state becomes unstable close to half filling and the compressibility jumps to negative values in the bad metal state. Concomitantly, C/C_0 is pushed to a value well above 1 which is easily understood from Eq. (14) for the parameter regime where the right hand side (rhs) is still positive (cf. Fig. 8(a)).

For $U \gtrsim U_{\text{CEP}}$ the metallic state still persists in a small doping range with negative compressibility and the rhs of Eq. (14) is still positive (see the turquoise curve in Fig. 7 and the corresponding turquoise curve for C/C_0 in Fig. 8(b)). The turquoise circle represents an end point beyond which the capacitance is negative in a small doping range: When the bad metal state is stabilized at larger n , the inverse compressibility jumps to a more negative value. There the capacitance C becomes negative which signifies that the charging of the electrodes changes (negative C are not displayed in Fig. 8). We do not investigate that charging instability further in this work (it was discussed in Ref. [41]). Eventually, with a slightly higher filling, the negative inverse compressibility is again reduced sufficiently so that the rhs of Eq. (14) becomes positive again and the second branch of the (positive) capacitance curve close to half filling is observed.

Eventually, for U in the vicinity of U_c^* (see the purple curves in Figs. 7 and Fig. 8(b)), the rhs of Eq. (14) is zero twice in the regime of negative compressibility. Correspondingly, the capacitance diverges twice and it attains negative values around $n = 1.94$. For even stronger coupling the dip in the inverse compressibility is less pronounced and the capacitance displays a broader maximum (see the red and orange lines in Fig. 8(b) for $U = 2.0 W$ and $5.0 W$, respectively).

It is evident that, with the strong dependence of the capacitance on filling in the intermediate to strong coupling regime, switching capacitances through small electronic-density variations appears to be feasible.

Moreover, we suggest that with electric pulse switching between the high resistance Mott insulator and the low resistance metallic state [52] it is possible to switch between low and high capacitance in a corresponding device. This is indicated in Fig. 9 for the capacitance transition with $U/W = 1.6$.

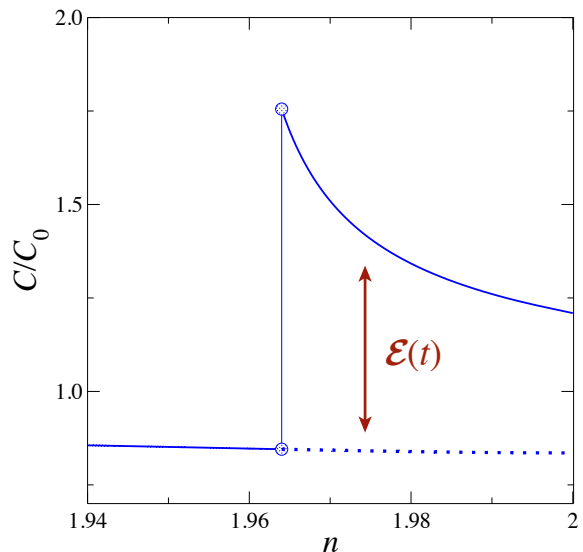


FIG. 9. Schematics of the capacitance switching induced by a short electric pulse $\mathcal{E}(t)$. The Hund's coupling is $J_H = W/6$ and $U = 1.6 W$. Below approximately $n \simeq 1.965$, the continuous blue line represents the capacitance with electrodes in the stable metallic state, whereas above $n \simeq 1.965$ this line refers to the stable bad metal state. The dotted blue line represents the metastable metallic case. The obtained effect is enhanced when approaching the transition, that is, when the energy difference between the two phases is smaller.

IV. BLUME-EMERY-GRIFFITHS APPROACH

The phase diagram of the two-band Hubbard model close to half-filling is surprisingly intricate exposing a first-order and a continuous phase transition (Figs. 2 and 4)—even though magnetic transitions are disregarded. The interpretation, however, is elusive as the slave-boson technique involves already seven bosonic fields in the paramagnetic state (at least four fields are relevant in the vicinity of half-filling) and their interplay jointly with the fermions is to be understood.

In the spirit of the Ising lattice-gas formulation of the liquid-gas transition we intend to mimic the bosonic fields by Ising-like pseudospins. The procedure builds on the assumption that it is not unreasonable to represent bosonic fields by classical fields and that the metal to bad metal transition is controlled by the bosonic degrees of freedom. For this purpose we simplify the formalism with exclusive focus on these transitions. We introduce a Blume-Emery-Griffiths (BEG) model [53] for the pseudospin degrees of freedom to better capture the machinery of the transition rather than gain quantitative results.

Such a simplification will not pave the way to reproduce the Mott transition or magnetic transitions close to half-filling. However it will generate qualitatively similar results as those in the previous section and thereby allows to understand the addressed transitions eventually in the more comprehensive framework of slave-boson theory.

A. BEG model and relation to the slave-boson representation

The basic idea is to interpret the bosonic degrees of freedom in terms of classical Ising-fields (pseudospins) which are controlled by various couplings. Foremost, there is a Zeeman-like coupling term which provides the energetical splitting between different configurations of doubly occupied sites, so that the Hund's coupling J_H becomes a pseudo magnetic field for the Ising fields. Then there is for sufficiently strong interaction U an effective nearest-neighbor exchange between orbital states of doubly occupied sites that is translated into an Ising-type nearest-neighbor coupling of the pseudospins.

The feedback of the Ising pseudo spins to the fermionic subsystem controls the kinetics of the fermions. It is the effective mass or rather the quasiparticle residue z^2 (see Eq. (A4)) through which the bosonic fields affect the kinetic fermionic term. We will use the dependency of z^2 on the bosonic fields, now for the dependence of z^2 on the classical Ising fields.

Yet there is a second (reverse) feedback mechanism: the fermionic degrees of freedom are expected to control the bosonic fields, that is, the Ising fields in this approach. With the fermions coupled to the pseudospins, the latter must necessarily fluctuate, even though they are introduced as classical fields. Although this is a rather crude approximation we introduce the effective bandwidth of the fermions as a soft energy cut-off for the fluctuations of the pseudo spins by implementation of this energy cut-off as an effective temperature for the pseudospins. In fact, we will see that this approximation reproduces the slave-boson results qualitatively.

In detail we now proceed as follows: In order to keep the number of pseudospin components minimal we only consider the fields related to the three doubly occupied states and the field representing the singly occupied sites. This will be sufficient for an intermediate coupling regime below half-filling (but above quarter filling). Later we will address the shortcomings of this reduction of degrees of freedom. Moreover one of the three fields representing doubly occupied sites may be related to the further fields through a constraint (see Eq. (B11)). Consequently we consider a spin-one Ising Hamiltonian for the pseudospins S_i . We identify $S_i = 1$ with the spin-parallel occupation of the two orbitals on a site i , i.e. with d_P^2 , and $S_i = -1$ with the spin-antiparallel occupation of the two orbitals, i.e. with d_A^2 . The singly occupied sites are represented by $S_i = 0$, which relates to the slave boson field p^2 on that site.

For arbitrary nearest-neighbor contributions the pseudospin representation of the bosonic degrees of freedom leads to a generalized form of the Blume-Emery-Griffiths (BEG) model [54]. We find that an antiferromagnetic nearest-neighbor (bilinear) Ising coupling is consistent with the slave-boson results; we will also provide a discussion for the choice of valid BEG-parameter regimes in Appendix E.

The Hamiltonian for the generalized BEG-model has the following structure for Ising spins on N_L sites with nearest-neighbor coupling:

$$\mathcal{H} = -\mathcal{J} \sum_{\langle i,j \rangle} S_i S_j - \mathcal{K} \sum_{\langle i,j \rangle} S_i^2 S_j^2 + \Delta \sum_{i=1}^{N_L} S_i^2 - h \sum_{i=1}^{N_L} S_i - \mathcal{L} \sum_{\langle i,j \rangle} (S_i S_j^2 + S_i^2 S_j) + E_0 \quad (15)$$

which is the most general Hamiltonian for three classical states per site and nearest-neighbor coupling [54]. Here \mathcal{J} is the coupling which controls ferromagnetic $\mathcal{J} > 0$ or antiferromagnetic $\mathcal{J} < 0$ correlations of the Ising pseudospins, that is, in the language of the two-band Hubbard model, it favors double occupancy with the same or different orbital states on neighboring sites, respectively. The ‘‘magnetic field’’ h aligns the pseudospins and corresponds to the Hund's coupling: $h = J_H/2$ (see Appendix E). The parameter $-\Delta$ in Eq. (15) controls the number of sites with zero pseudospin and is related to μ , the chemical potential. Therefore we refer to it as the chemical potential related to the pseudospin particles. It will be fixed by the filling n .

The coupling \mathcal{L} is to be included if the nearest-neighbor interaction strength in $d_P - d_P$ configurations and the strength in $d_A - d_A$ configurations is not equal (see Appendix E). Here we refer to a $d_{P/A} - d_{P/A}$ configuration when two neighboring sites are both occupied by a $d_{P/A}$ boson. Obviously, such terms with finite \mathcal{L} denote in mean-field theory a shift of both h and Δ proportional to $\mathcal{L}\langle S_i^2 \rangle$ and to $-\mathcal{L}\langle S_i \rangle$, respectively. In that respect, the coupling \mathcal{L} is not relevant for the existence of the discussed transition although it renormalizes the other couplings. In this section we only consider the BEG-model [53] where $\mathcal{L} = 0$ and address finite \mathcal{L} in Appendix E.

As to the fermionic dispersion, Eq. (8a), the z^2 -factor is reduced to

$$z^2 = \frac{4p^2 (d_P + d_A + d_H)^2}{1 - \left(\frac{2-n}{2}\right)^2} \quad (16)$$

in the approach with only four bosonic degrees of freedom (cf. Eq. (13), where the triple occupation was included for a better quantitative estimate of the compressibility). We stay below half-filling ($n < 2$) because the corresponding results above half-filling may be derived directly from particle-hole symmetry, and we introduce $\delta = 2 - n$ as the doping parameter. The relative number of singly occupied sites is $4p^2 = \delta$ which in BEG is the relative number of zero-spin sites. Here, the factor 4 accounts for the two-spin directions and the two orbitals per site. The bosonic field d_H^2 is fixed by the relation (B11). As in BEG the d_P and d_A configurations are assigned to spin 1 and spin -1 , respectively, one immediately identifies

$$\langle S_i \rangle = 2d_P^2 - 2d_A^2 \equiv m \quad (17a)$$

$$\langle S_i^2 \rangle = 2d_P^2 + 2d_A^2 \equiv q \quad (17b)$$

where we introduced the standard BEG-notation for the mean-field values of S_i and S_i^2 , that is, m and q , viz. pseudospin magnetization and relative number of sites with pseudospin 1. Filling is expressed by $n = 1 + 2d_P^2 + 2d_A^2 + 2d_H^2$ if only four bosonic fields are considered and this expression may be rewritten as

$$q = 1 - \delta - 2d_H^2. \quad (18)$$

To include the field d_H^2 through a constraint is consistent with the counting, however the sites with d_H -

configuration are not represented by a proper term in the Hamiltonian. This approach is justified if the number of such sites, that is d_H^2 , is much smaller than d_P^2 , d_A^2 and doping δ which is true close to the considered transition (see the results below). One may introduce an on-site energy for the sites with d_H -configuration but this accounts just for a shift of the chemical potential Δ and of the coupling constant \mathcal{K} which does not affect our mean-field results qualitatively.

It is straightforward to derive from Eqs. (B11), (16) and (18) the following expression

$$z^2(m, q) = \frac{1}{2} \frac{(1 - q^2 - 2d_H^2)(q + 2d_H^2 + \sqrt{q^2 - m^2} + 2d_H(\sqrt{q+m} + \sqrt{q-m}))}{1 - \frac{1}{4}(1 - q - 2d_H^2)^2} \quad (19)$$

where

$$d_H^2(m, q) = \frac{1}{4} \frac{q^2 - m^2}{13q + 5m - 12\sqrt{q^2 - m^2}}. \quad (20)$$

The variables q and m are taken from the mean-field solutions of the BEG model. The filling n is found parametrically from

$$n(m, q) = 1 + q + 2d_H^2(m, q) \quad (21)$$

which is equivalent to Eq. (18).

It is convenient to determine the upper and lower bounds for z^2 :

$$\frac{1}{2} f(\delta) \leq z^2 \leq \frac{3}{2} f(\delta) \quad \text{with} \quad f(\delta) = \frac{\delta(1-\delta)}{1 - \frac{1}{4}\delta^2} \quad (22)$$

which is valid for the considered case of four distinct on-site states. The lower bound is derived from full polarization, that is $m = q$ which implies $d_A^2 = 0 = d_H^2$ and $2d_P^2 = 1 - \delta$. The upper bound is the ‘‘non-magnetic’’ state with $m = 0$ which implies $2d_A^2 = 2d_P^2 = 2d_H^2 = (1/3)(1 - \delta)$.

The BEG mean-field free energy F of the paramagnetic state in the presence of finite field h is (see Refs. [53, 54]):

$$F(T, h, \Delta)/N_L = \frac{1}{2}\zeta\mathcal{J}m^2 + \frac{1}{2}\zeta\mathcal{K}q^2 + k_B T \ln \left[1 + 2e^{-\frac{(\Delta - \zeta\mathcal{K}q)}{k_B T}} \cosh \frac{\zeta\mathcal{J}m + h}{k_B T} \right] \quad (23)$$

where ζ is the number of nearest-neighbor sites. We may cast the mean-field equations $\partial F/\partial m = 0$ and $\partial F/\partial q = 0$ into the form:

$$h = -\zeta\mathcal{J}m + \frac{k_B T}{2} \ln \frac{q+m}{q-m} \quad (24)$$

$$\Delta = \zeta\mathcal{K}q - \frac{k_B T}{2} \ln \frac{q^2 - m^2}{4(1-q)^2} \quad (25)$$

For such a classical Ising-type model a zero-temperature evaluation produces phase transitions where m and q change discontinuously (see, e.g., Fig. 2 in Ref. 54). This is not necessarily expected for the concomitant bosonic fields d_P and d_A (see Figs. 5(a) and (b) above) that are related to m and q through the identification (24) and (25). These bosonic fields are in fact enslaved by the fermionic degrees of freedom and the challenge is then to allow for a control of the pseudospins through the fermions, at least approximately. We achieve this through a feedback mechanism where we assume that the temperature of the pseudospin BEG-system is an effective temperature which is proportional to some power α of the fermionic bandwidth: $k_B T_{\text{eff}} = g_{\text{fb}} z^{2\alpha}$. Here g_{fb} is a (fermion-boson) coupling constant which however depends on α and will be discussed below.

The excitations of the bosonic system involve fermionic Greens functions (or rather spectral functions) which are weighted by z^2 . As virtual particle-hole excitations couple to the bosonic (pseudospin) degrees of freedom, one may assume in view of a perturbative approach that $\alpha = 2$ is a suitable choice. For strong coupling, that is $t \ll U$, this may not be valid anymore and it may be argued that the excitations exist in an energy window given by the bandwidth $z^2 W$. Accordingly, one would then rather switch to $\alpha = 1$ with increasing coupling. So far there is no microscopic scheme how to determine T_{eff} and α [55]. We find that the choice $\alpha = 1$ does not produce a discontinuous transition. Here we investigate the case with $\alpha = 2$ which allows to reproduce the slave-boson results qualitatively when \mathcal{J} is chosen appropriately. Consequently we introduce the effective temperature of the pseudospin system through

$$k_B T_{\text{eff}} = g_{\text{fb}} \cdot z^4 \quad (26)$$

where z^2 is a function of m and q (see Eq. (19)) and the fermion-boson coupling g_{fb} is chosen such that we recover the position of the jump or inflection point of z^2 in dependence on filling n of the slave-boson results. This filling

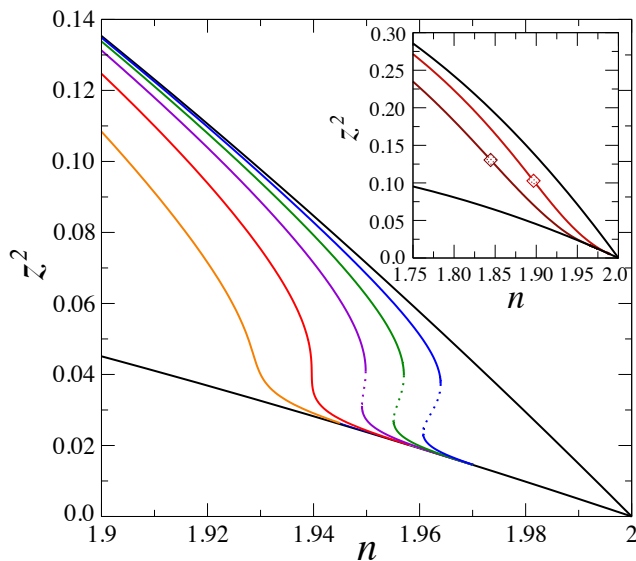


FIG. 10. Quasiparticle residue from BEG evaluation. The black lines are the upper and lower bounds for z^2 from Eq. (22). Parameters are $\mathcal{J} = -0.7$ and $g_{\text{fb}} = 90$ (orange), $\mathcal{J} = -0.5$ and $g_{\text{fb}} = 180$ (light red), $\mathcal{J} = -0.3$ and $g_{\text{fb}} = 330$ (magenta), $\mathcal{J} = 0.0$ and $g_{\text{fb}} = 580$ (green), $\mathcal{J} = 0.5$ and $g_{\text{fb}} = 1100$ (blue). All energies are in units of $J_{\text{H}}/2$ and $h = 1.0$. Inset: $\mathcal{J} = -1.0$, $h = 1.0$, $g_{\text{fb}} = 50$ (red) and $g_{\text{fb}} = 20$ (dark red). The two diamonds mark the respective inflection points.

is denoted by n_0 . We emphasize that this pseudospin approach to the bosonic fields is necessarily a phenomenological approach where the “temperature profile”, that is, the dependence of the pseudospin temperature T_{eff} on n (expressed through $q(n)$ and $m(n)$) is controlled by the strength of the coupling parameter g_{fb} and the effectiveness of the feedback mechanism, determined by the exponent α .

It is evident that in the limit of half-filling, T_{eff} converges to zero as z^2 approaches zero. This reproduces the correct limits of the fields d_{P} , d_{A} and d_{H} but we do not consider this pseudospin approach as appropriate to discuss the Mott transition. We rather discuss the results below half-filling where our approach provides a transition to a state with negative compressibility in line with the slave-boson results.

B. Results from the BEG approach and interpretation

The procedure to calculate z^2 in dependence on n is as follows: We gain m from the mean-field equation (24) for given q , whereby we replace the temperature by the effective temperature T_{eff} from Eq. (26). Then we use relations (19) and (20) to determine z^2 . We plot z^2 in dependence on filling n which is given by Eq. (21).

Most strikingly, z^2 displays a transition in this evaluation with BEG Ising-type fields, the nature of which

depends on the strength of nearest neighbor coupling \mathcal{J} with respect to $h = J_{\text{H}}/2$ (see Fig. 10). We consider all energies in this section in units of $J_{\text{H}}/2$. The coupling parameter g_{fb} mostly shifts the curves but does not affect the transition qualitatively; its role will be discussed below.

These results are consistent with those of the slave-boson evaluation (SB) in the previous section in the sense that we find a continuous as well as a discontinuous transition in a doping regime close to half-filling. In SB the type of transition is controlled by the correlation strength U/W (see Fig. 1). Here the transition is tuned by \mathcal{J} and \mathcal{L} . The dependence of \mathcal{J} , \mathcal{K} and \mathcal{L} on the Hubbard-model parameters U , t , t' and J_{H} is rather complex, and we only estimate the relative size of the BEG-parameters in Appendix E.

Before we suggest an interpretation of the filling dependence of z^2 we briefly discuss the coupling parameter g_{fb} . As said this parameter shifts the inflection point or the jump in z^2 : the lower the value of g_{fb} the farther away the inflection point from half-filling (this is exemplified in the inset of Fig. 10). In few of the SB results it appears that g_{fb} is inverse to U . This is not unreasonable as a larger g_{fb} , that is, a higher energy cut-off $k_{\text{B}}T_{\text{eff}}$ accounts for stronger fluctuations in the pseudospin field. Conversely, one expects that for larger U the slave boson fields are more tightly bound to the fermionic degrees of freedom and fluctuations of the fields are suppressed. We introduced g_{fb} phenomenologically and we just use it to shift the transition structure of z^2 to a position compatible with the SB result.

The values of g_{fb} in Fig. 10 are surprisingly large. A brief analysis relates these large values to the smallness of z^4 . To understand this argument, we reparametrize the fermion-boson coupling g_{fb} in terms of a temperature T_0 and a $z_0^2 = z^2(m_0, q_0)$:

$$k_{\text{B}}T_{\text{eff}}(m, q) = g_{\text{fb}} z^4(m, q) = \frac{k_{\text{B}}T_0}{z_0^4} z^4(m, q) \quad (27)$$

whereby q_0 is a reference value which we will choose appropriately and m_0 is calculated from the mean-field equation (24) with m , q and T replaced by m_0 , q_0 and T_0 . We choose the reference value q_0 such that $q_0 = n_0 - 1 - 2d_{\text{H}}^2$ holds (see Eq. (18)) where we can neglect the small contribution of d_{H}^2 for an approximate specification of q_0 in the regime close to half-filling. Now with given q_0 and the requirement that the inflection point or jump of z^2 is placed in the range of fillings consistent with SB results one identifies values of $k_{\text{B}}T_0$ in the range of 0.2 – 0.4 and through the relation (27) one finds g_{fb} in the range of 20 – 1100. The smallness of z_0^4 requires large values of g_{fb} in order to fulfill $g_{\text{fb}} = (k_{\text{B}}T_0/z_0^4)$.

Qualitatively, the z^2 -curves of Fig. 10 resemble those of the SB result in Fig. 1. One might object that z^2 calculated within SB theory is notably larger in the metallic regime, especially for $U < W$. This discrepancy, however, is not a consequence of the BEG Ising-type evaluation but it is caused mainly by the neglect of triple

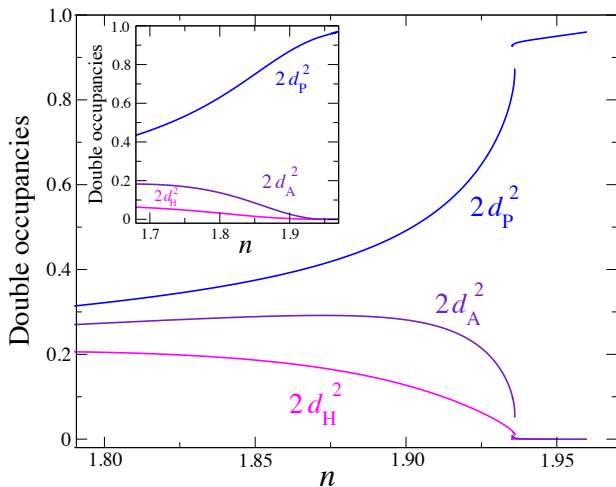


FIG. 11. Bosonic occupations $2d_P^2$, $2d_A^2$, and $2d_H^2$ in dependence on filling n . The BEG parameters are $h=1.0$, $\mathcal{J}=-0.3$, and $g_{fb}=330$. Inset: $h=1.0$, $\mathcal{J}=-1.0$, and $g_{fb}=20$.

occupancies. In fact, the bounds of Eq. (22) (see the black curves in Fig. 10) also hold for the SB evaluation if triple occupancies and empty sites are excluded. These neglected contributions are sizable for small and intermediate values of U whereas we are targeting the regime of larger values of U in the BEG scheme.

The down bending or the jump of z^2 to low values close to half-filling is caused by the strong increase of the “BEG-magnetization” m in a regime where q approaches one. The upper bound in Eq. (22) stands for $m=0$ whereas the lower bound is determined by full polarization $m=q$. Correspondingly, in the language of the two-band Hubbard model, we observe a transition from a state with smaller orbital polarization ($d_H^2 < d_A^2 < d_P^2$) to a state with strong orbital polarization close to half-filling: $d_H^2 \simeq 0 \simeq d_A^2$ and $2d_P^2 \gtrsim 1 - \delta$ (see Fig. 11 for the BEG result of the filling dependence of $2d_{P,A,H}^2$). Again, the filling dependence of these occupations is qualitatively similar to what was found in the SB evaluation. That inspires the following interpretation of the result of the two-band Hubbard model:

Obviously, a finite Hund’s coupling favors a double occupation of sites where the spins of the two orbitals are aligned (d_P -state). For strong coupling bosonic fluctuations to $d_{A,H}$ states are reduced—this is expressed here through a stronger fermion-boson coupling, that is, through a smaller g_{fb} which entails a smaller effective temperature for the fluctuations in our pseudospin evaluation. Then, the pseudospin magnetization m is larger. Correspondingly $2d_P^2$ is larger and $2d_{A,H}^2$ are smaller for stronger electronic correlations. However there is a further impact of strong coupling: an orbital (antiferromagnetic) nearest neighbor coupling $\mathcal{J} < 0$ becomes effective which induces local fluctuations to states with antiparallel spins on the two orbitals of a site. These fluctuations prevent a sharp transition to an orbitally polarized state: we only observe an inflection point in $z(n)^2$.

For intermediate coupling g_{fb} is larger and, correspondingly, the transition is closer to half-filling. Moreover, the reduced antiferromagnetic (orbital) coupling \mathcal{J} allows Hund’s coupling to dominate in this regime and we identify a discontinuous transition in $z(n)^2$.

In SB theory all single-site double occupancies are represented by bosons, the fluctuations of which are effectively the incoherent background to the (fermionic) quasiparticle excitations. It depends on the interplay of the fermions and the incoherent (bosonic) background if the reduction of z^2 is continuous or discontinuous.

C. Compressibility

The inverse compressibility is identified from the sum of the inverse compressibilities of the subsystems whereby each subsystem is characterized by its respective free energy (see, for example, Ref. [41]). Each of the free energy terms yields an additive contribution to the inverse compressibility κ^{-1} when forming the second derivative with respect to the total density (and multiplying by a factor density squared). As we keep volume and number of lattice sites N_L constant we can use the filling n instead of the density in our evaluation. There is a fermionic free energy term, which is in fact the fermionic kinetic energy controlled by the inverse effective mass $z^2(n)$, and a pseudospin free energy term originating from the BEG Hamiltonian.

In an approximation where d_H^2 is zero we find the simple relation $n = 1 + q$ and we can take the derivatives of the pseudospin free energy simply with respect to q to calculate the inverse compressibility. With inclusion of a finite d_H^2 , we have to respect the relation (21): correspondingly there are corrections from the derivative

$$dn/dq = 1 + 2d(d_H^2)/dq \quad (28)$$

that can be sizable because d_H^2 decreases rapidly in the doping regime of the continuous transition.

Here the compressibility is to be determined not for given orbital polarization m but for fixed Hund’s coupling, that is, for fixed field h . As regards the other BEG-variable, q , this is the variable which is related to filling as just discussed. So the appropriate pseudospin free energy depends on h and q which is a Legendre transform of $F(h, \Delta)$ of Eq. (23) from Δ to q which we denote as $\Gamma(h, q)$. The derivative of $\Gamma(h, q)/N_L$ with respect to q naturally yields $-\Delta(h, q)$, which may be interpreted as the chemical potential related to the q -particles. However, as we actually have to take the derivative of $\Gamma(h, q)$ with respect to n and not q , we have to multiply the q -derivative of $\Gamma(h, q)$ by dq/dn :

$$\frac{d(\Gamma/N_L)}{dn} = -\Delta / (1 + 2 \frac{d(d_H^2)}{dq}) \quad (29)$$

where all terms depend through q on n . The contribution of the pseudospins to the inverse compressibility, κ_{ps}^{-1} , is

now the derivative of this pseudospin chemical potential with respect to n :

$$(n^2 \kappa_{\text{ps}})^{-1} = \frac{d^2(\Gamma/N_L)}{dn^2} = -\frac{d}{dn} \left(\Delta / \left(1 + 2 \frac{d(d_H^2)}{dq} \right) \right) \quad (30)$$

Here $\Delta(h, q)$ is found from the mean-field expression Eq. (25) with m replaced by its q -dependent mean-field value $m(q)$, and the temperature is replaced by T_{eff} of Eq. (27) in that mean-field evaluation. It is evident that the n -dependence of the term in parentheses on the rhs of Eq. (30) has to be determined first from Eq. (21) and the mean-field equations, before the derivative with respect to n can be calculated.

The fermionic contribution to the inverse compressibility, κ_{qp}^{-1} , results directly from the second derivative of the kinetic energy $z(n)^2 E_{\text{kin}}(n)$ with respect to n . In order to have a simple analytical expression for $E_{\text{kin}}(n)$ we take the dispersion from Eq. (2) with $t' = 0$. As the second derivative of the kinetic energy is dominated by the curvature of $z(n)^2$ in the transition regime, the filling dependence of the unrenormalized $E_{\text{kin}}(n)$ is of little consequence if it is sufficiently smooth. This is the case, as the dispersion integrates to the smooth function $E_{\text{kin}}(n)/N_L = -\frac{2}{\pi} W \cos[\frac{\pi}{4}(2-n)]$ (compare Eq. (11) where W is the bandwidth and the two spin directions have been taken care of by a factor 2. The fermionic compressibility is now

$$(n^2 \kappa_{\text{qp}})^{-1} = \frac{d^2(z^2 E_{\text{kin}}/N_L)}{dn^2} \quad (31)$$

In order to put κ_{qp}^{-1} in relation to κ_{ps}^{-1} quantitatively, we have to fix W : with $J_H = W/6$ used in the section on the SB results and $h = J_H/2$, we choose correspondingly $W = 12h$ for the further evaluation of the total compressibility.

Eventually, the total compressibility κ_{tot} is determined from the subsystem compressibilities Eqs. (30) and (31) through

$$\kappa_{\text{tot}}^{-1} = \kappa_{\text{ps}}^{-1} + \kappa_{\text{qp}}^{-1} \quad (32)$$

As is obvious from Eq. (30) we now need Δ which is extracted from Eq. (25) where T has to be replaced by T_{eff} . The evaluation of Δ requires to choose an appropriate \mathcal{K} -parameter of the BEG-model. As one can learn from Eqs. (E2) in Appendix E and the following discussion, the parameter \mathcal{K} is positive and considerably larger than $|\mathcal{J}|$. We take $\mathcal{K} = 8.0$ (again in units of J_H).

The compressibilities are displayed in Fig. 12 for $\mathcal{J} = -1.0$. That value of \mathcal{J} signifies that the transition in $z^2(n)$ is continuous. This is now reflected in a continuous transition of the compressibility κ_{tot} from positive to negative values close to half-filling.

Similarly, the compressibilities are discontinuous for $\mathcal{J} = -0.3$ as seen in Fig. 13. This is expected as the quasiparticle weight z^2 is discontinuous for these less negative values of \mathcal{J} .

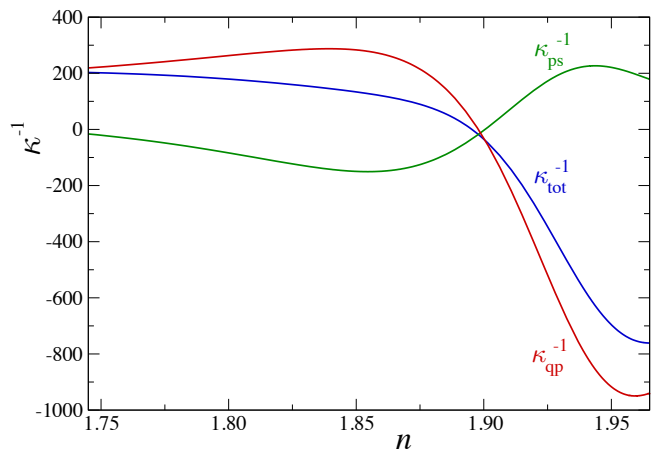


FIG. 12. Compressibility in dependence on filling n . The BEG parameters are $h=1.0$, $\mathcal{J}=-1.0$, $g_{\text{fb}}=50$ and $\mathcal{K}=8.0$. Here κ^{-1} is in units of $J_H/2a^2$ and the coupling parameters are in units of $J_H/2$.

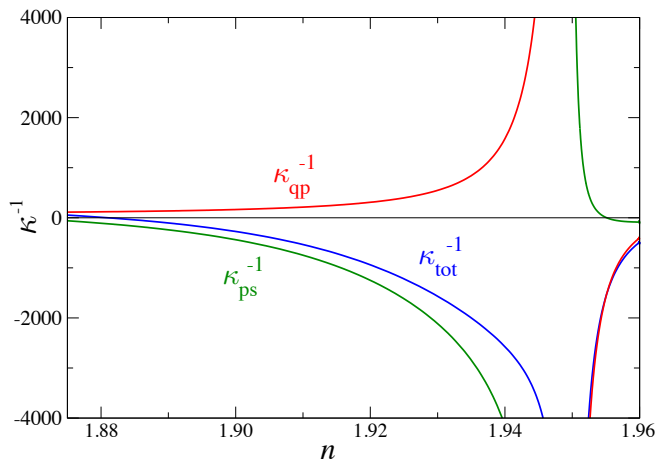


FIG. 13. Compressibility in dependence on filling n . The BEG parameters are $h=1.0$, $\mathcal{J}=-0.3$, $g_{\text{fb}}=330$ and $\mathcal{K}=8.0$. Here κ^{-1} is in units of $J_H/2a^2$ and the coupling parameters are in units of $J_H/2$.

It is obvious that in the considered filling regime the inverse pseudospin compressibility κ_{ps}^{-1} partially cancels the inverse quasiparticle compressibility κ_{qp}^{-1} . The exact degree of cancellation depends on the relative values of the partial compressibilities. However in the vicinity of the transition, κ_{qp}^{-1} becomes already negative when κ_{ps}^{-1} is still negative (see Fig. 12). This behavior is analogous to what was observed in the SB formalism for κ_{f}^{-1} and κ_{b}^{-1} . If the zero crossings of both were at the same filling n then the transition to bad metal behavior (the inflection point of z^2) would coincide with the transition to negative compressibility. Instead we find two distinct transitions.

The negative compressibility of the pseudospin subsystem indicates that it is not in its (thermodynamic) equilibrium which is presumably true also for the bosonic sub-

system in SB theory—however, a partition into subsystems is not evident there. For the pseudospin subsystem we find a mean-field solution for given q and the appropriate effective temperature but this solution does not represent the global minimum for $q > 0.744$ (assuming here $\mathcal{J} = -1.0$). The chemical-potential parameter $-\Delta$ of Eq. (25) is tied to the pseudospin field q , which is fixed by the choice of n . Actually a considerably lower q represents the thermodynamically stable state for that value of Δ . If n and, correspondingly, q were not fixed then the pseudospin system would relax to this lower q . The thermodynamic stability of the BEG subsystem is discussed in Appendix F. It is the requirement of sufficiently large q to obtain a filling in the low doping regime and of sufficiently small effective temperature T_{eff} enforced by small values of z^2 close to half filling that drives the pseudospin out of equilibrium: there is no global minimum of the thermodynamic potential in this regime.

Close to half-filling κ_{ps}^{-1} becomes positive for $\mathcal{J} = -1.0$ (see Fig. 12). This behavior close to the metallic transition is triggered by the strong filling dependence of the fields that represent double occupancies. In particular the field d_{H}^2 enters through the factor dq/dn of Eq. (28) into Eq. (29) and reverses the slope of the pseudospin chemical potential term $d(\Gamma/N_{\text{L}})/dn$ with respect to n in the bad metal state. This signifies that κ_{ps}^{-1} is positive there. However, the pseudospin subsystem is still not in its (thermodynamic) equilibrium.

For the discontinuous case (see Fig. 13) κ_{ps}^{-1} becomes again negative in the vicinity of half-filling as opposed to the behavior of κ_{b}^{-1} in the SB evaluation. In this respect we reemphasize that the BEG-results cannot be trusted for lower values of U/W . In fact, effective interactions between doubly occupied sites were parameterized as nearest neighbor pseudospin exchange within a perturbative scheme where triple and quadruple occupancies are suppressed. On the other hand, if $U \gg J_{\text{H}}$ the on-site energies of the different configurations with double occupancy approach each other and the sites with finite d_{H}^2 would have to be considered also explicitly in the Hamiltonian as their relative number cannot be neglected there. Consequently, we expect a parameter window for intermediate to moderately strong correlation strength where the results from this phenomenological approach are qualitatively valid.

Overall the results from the BEG modeling can be compared reasonably well with those of the SB theory. They explain the transition in $z^2(n)$ through a transition in the pseudospin magnetization controlled by h , that is, in the orbital polarization of the 2-band Hubbard model controlled by J_{H} . Also the transition to the negative compressibility in the low doping regime is recovered. However, it is not a phase transition of the pseudospin system of the BEG model but it is the feedback mechanism between the pseudospin system and the (fermionic) quasiparticle system which causes the transitional behavior.

V. SUMMARY AND OUTLOOK

This work is concerned with the two-band Hubbard model in the presence of a finite Hund's coupling J_{H} . In particular, we investigated the paramagnetic state close to half filling ($n = 2$) using an extended Kotliar-Ruckenstein slave-boson technique. Previously, a first order transition with a coexistence regime between a metallic and a bad metal state below a critical point (CP) was identified [27] and, more recently, a continuous transition signaling a charge instability for larger on-site interaction U was discovered [28]. Both transitions were considered in dependence on J_{H}/U and it was found that they are absent for $J_{\text{H}} = 0$.

In this paper we analyzed these transitions jointly for fixed J_{H} and found that the line related to the continuous transition, characterized by zero inverse compressibility, merges with the first order transition at a critical end point (CEP). This CEP is close to the CP. Beyond the CEP, that is for the filling range towards half filling, the charge instability persists, however only in the metallic state which is not the global free energy minimum in this range of n . Rather the inverse compressibility jumps from positive to negative values jointly with the inverse effective mass along the first order transition line. This transition into the negative-compressibility bad-metal regime extends to smaller values of U down to the metal-insulator transition at half filling where it ends at the Mott-insulator transition for the two-band Hubbard model.

The slave boson theory suits well to distinguish between the excitations into coherent (fermionic) quasiparticles and multiparticle or collective (bosonic) excitations. Even though this is implemented here only on the saddle point level, the decomposition allows in this context to study the quasiparticle contribution to the compressibility separately from the bosonic background as the inverse compressibility can be split into the corresponding partial (inverse) compressibilities. The quasiparticle compressibility is controlled by the curvature and jump of the inverse effective mass $\propto z^2(n)$. In contrast, the bosonic contribution in this regime is governed by the bosonic field which represents doubly occupied sites with parallel spins in the two distinct orbitals, that is, $d_{\text{P}}^2(n)$. The Hund's coupling J_{H} triggers both, the sharp drop in $z^2(n)$ and the steep increase in the double occupancy $d_{\text{P}}^2(n)$ when approaching half filling. This drop and increase for $z^2(n)$ and $d_{\text{P}}^2(n)$, respectively, may be realized by a jump or an inflection point in their n -dependence. Obviously, Hund's coupling favors this type of double occupancy (d_{P}^2) energetically thereby suppressing not only the competing double occupancy configurations but also the triple occupancy and concomitantly the single occupancy so effectively that a phase transition is accomplished—either first order or continuous.

We confirmed that in the absence of Hund's coupling, the curvature of $z^2(n)$ close to half filling does not switch its sign, i.e., $z^2(n)$ stays concave. The filling range where

$z^2(n)$ becomes convex, which signals a charge instability and negative compressibility, is in fact controlled by the size of J_H .

In a toy-model approach, the most prominent bosonic degrees of freedom were mapped onto Ising-like (spin-1) pseudospins within a Blume-Emery-Griffiths model that implements the Hund's coupling by a Zeeman-like field and the correlations through quadratic and bi-quadratic nearest-neighbor exchange-energy terms. This allows to discuss these degrees of freedom in a classical model although the Ising fields are then coupled to the (fully quantum mechanical) quasiparticle system through a feedback mechanism. It appears in this approximate treatment that the transition is not a phase transition of the pseudospin system itself but it is a transition generated by the feedback of the quasiparticles and vice versa. The pseudospin system by itself is rather out of equilibrium close to half filling and the coupling to the fermionic system keeps it in this state. It is only the joint pseudospin-quasiparticle system that, for fixed filling n , is in equilibrium.

The capacitance of a heterostructure device is intimately related to electronic compressibilities of the elec-

trodes [41]. As the compressibility of this two-band Hubbard-model electronic system depends very sensitively on the electron density close to half filling—also under the consideration of the transitions to negative compressibility—it is well conceivable that micro-device capacitances may be very effectively controlled and switched through small electronic-density variations.

We also suggest the intriguing possibility to switch between low and high capacitance through electric pulse switching between the high resistance Mott insulator and the low resistance metallic state [52].

ACKNOWLEDGMENTS

Financial support by the Deutsche Forschungsgemeinschaft (project number 107745057, TRR 80) is gratefully acknowledged. R.F. is grateful for the warm hospitality at University of Augsburg where part of this work has been done, and to the Région Normandie for financial support.

-
- [1] Patrik Fazekas, *Lecture Notes on Electron Correlation and Magnetism* (World Scientific, Singapore, 1999).
- [2] P. W. Anderson, *Science* **235**, 1196 (1987).
- [3] M. R. Norman, *Science* **332**, 196 (2011).
- [4] D. J. Scalapino, *Rev. Mod. Phys.* **84**, 1383 (2012).
- [5] B. Keimer, S. A. Kivelson, M. R. Norman, S. Uchida, and J. Zaanen, *Nature* **518**, 179 (2015).
- [6] J. Hubbard, *Proc. Royal Soc. Lond. A* **276**, 238 (1963).
- [7] M. Gutzwiller, *Phys. Rev. Lett.* **10**, 159 (1963).
- [8] W. F. Brinkman and T. M. Rice, *Phys. Rev. B.* **2**, 4302 (1970).
- [9] J. Kanamori, *Prog. Theor. Phys.* **30**, 275 (1963).
- [10] J. P. Lu, *Phys. Rev. B* **49**, 5687 (1994).
- [11] R. Frésard and G. Kotliar, *Phys. Rev. B* **56**, 12 909 (1997).
- [12] F. Lechermann, A. Georges, G. Kotliar, and O. Parcollet, *Phys. Rev. B* **76**, 155102 (2007).
- [13] V.I. Anisimov, I.A. Nekrasov, D.E. Kondakov, T.M. Rice, and M. Sigríst, *Eur. Phys. J. B* **25**, 191 (2002).
- [14] A. Rüegg, M. Indergand, S. Pilgram, and M. Sigríst, *Eur. Phys. J. B* **48**, 55 (2005).
- [15] S. Biermann, L. de' Medici, A. Georges, *Phys. Rev. Lett.* **95**, 206401 (2005).
- [16] A. Liebsch, *Phys. Rev. Lett.* **95**, 116402 (2005).
- [17] A. Koga, K. Inaba, N. Kawakami, *Prog. Theor. Phys. Suppl.* **160**, 253 (2005).
- [18] T. Hotta and E. Dagotto, *Phys. Rev. Lett.* **92**, 227201 (2004).
- [19] R. Frésard, M. Raczkowski, and A. M. Oleś, *Phys. Stat. Sol. (b)* **242**, 370 (2005).
- [20] M. Raczkowski, R. Frésard, and A. M. Oleś, *Phys. Rev. B* **73**, 094429 (2006).
- [21] Ya-Min Quan, Da-Yong Liu, Hai-Qing Lin, Liang-Jian Zou, *J. Magn. Magn. Mater.* **456**, 329 (2018).
- [22] Y. Núñez-Fernández, G. Kotliar, and K. Hallberg, *Phys. Rev. B* **97**, 121113(R) (2018).
- [23] N. Aucar Boidi, H. Fernández García, Y. Núñez-Fernández, and K. Hallberg, *Phys. Rev. Research* **3**, 043213 (2021).
- [24] P. Werner, E. Gull, M. Troyer, and A. J. Millis, *Phys. Rev. Lett* **101**, 166405 (2008).
- [25] L. Fanfarillo and E. Bascones, *Phys. Rev. B* **92**, 075136 (2015).
- [26] K. M. Stadler, G. Kotliar, A. Weichselbaum, and J. von Delft, *Ann. Phys.* **405**, 365 (2019).
- [27] R. Frésard and M. Lamboley, *J. Low Temp. Phys.* **126**, 1091 (2002).
- [28] L. de' Medici, *Phys. Rev. Lett.* **118**, 167003 (2017).
- [29] A. Liebsch, *Phys. Rev. B* **77**, 115115 (2008).
- [30] J. P. Eisenstein, L. N. Pfeiffer, and K. W. West, *Phys. Rev. Lett.* **68**, 674 (1992); *Phys. Rev. B* **50**, 1760 (1994).
- [31] S. V. Kravchenko, V. M. Pudalov, and S. G. Semenchinsky, *Phys. Lett. A* **141**, 71 (1989).
- [32] S. Shapira, U. Sivan, P. M. Solomon, E. Buchstab, M. Tischler, and G. Ben Yoseph, *Phys. Rev. Lett.* **77**, 3181 (1996).
- [33] L. Li, C. Richter, S. Paetel, T. Kopp, J. Mannhart, and R. C. Ashoori, *Science* **332**, 825 (2011).
- [34] V. Tinkl, M. Breitschaft, C. Richter, and J. Mannhart, *Phys. Rev. B* **86**, 075116 (2012).
- [35] A. M. J. Schakel, *Phys. Rev. B* **64**, 245101 (2001).
- [36] D. Vollhardt, *Rev. Mod. Phys.* **56**, 99 (1984).
- [37] R. Frésard, K. Steffen, and T. Kopp, *Proc. of the 18th International Conference on Recent Progress in Many-Body Theories (MBT18)*, Niagara Falls (2015), *J. Phys.: Conf. Ser.* **702**, 012003 (2016).
- [38] K. Steffen, R. Frésard, and T. Kopp, *Phys. Rev. B* **95**,

035143 (2017).

[39] R. Frésard, M. Dzierzawa, and P. Wölfle, *Europhys. Lett.* **15**, 325 (1991).

[40] J. Seufert, D. Riegler, M. Klett, R. Thomale, and P. Wölfle, *Phys. Rev. B* **103**, 165117 (2021).

[41] T. Kopp and J. Mannhart, *J. Appl. Phys.* **106**, 064504 (2009).

[42] S. T. F. Hale and J. K. Freericks, *Phys. Rev. B* **85**, 205444 (2012).

[43] James K. Freericks, *Transport in Multilayered Nanostructures*, 2nd ed. (Imperial College Press, London, 2016).

[44] S. Sugano, Y. Tanabe, and H. Kamimura, *Multiplets of Transition-Metal Ions in Crystals*, Pure and Applied Physics **33**, Academic Press, New York (1970).

[45] J. Bünnemann, W. Weber, and F. Gebhard, *Phys. Rev. B* **57**, 6896 (1998).

[46] G. Kotliar and A.E. Ruckenstein, *Phys. Rev. Lett.* **57**, 1362 (1986).

[47] R. Frésard and T. Kopp, *Nucl. Phys. B* **594**, 769 (2001).

[48] R. Frésard, H. Ouerdane, and T. Kopp, *Nucl. Phys. B* **785**, 286 (2007).

[49] R. Frésard and T. Kopp, *Ann. Phys. (Berlin)* **524**, 175 (2012).

[50] C. Piefke and F. Lechermann, *Phys. Rev. B* **97**, 125154 (2018).

[51] C. Berthod, H. J. Zhang, A. F. Morpurgo, and T. Giamarchi, *Phys. Rev. Research*, **3**, 043036 (2021).

[52] L. Cario, C. Vaju, B. Corraze, V. Guiot, and E. Janod, *Adv. Mater.* **22**, 5193 (2010).

[53] M. Blume, V. J. Emery, and R. B. Griffiths, *Phys. Rev. A* **4**, 1071 (1971).

[54] Y. Saito, *J. Chem. Phys.* **74**, 713 (1981).

[55] One may expect that the energy scale T_{eff} results from a RG-type evaluation.

[56] N. Read, D. M. Newns, *J. Phys. C* **16**, L1055 (1983).

[57] N. Read, D. M. Newns, *J. Phys. C* **16**, 3273 (1983).

[58] D. M. Newns and N. Read, *Adv. in Physics* **36**, 799 (1987).

[59] R. Frésard, J. Kroha, and P. Wölfle, in *Theoretical Methods for Strongly Correlated Systems*, edited by A. Avella and F. Mancini, Springer Series in Solid-State Sciences Vol. 171 (Springer-Verlag, Berlin, 2012), pp. 65-101.

[60] V. H. Dao and R. Frésard, *Ann. Phys. (Berlin)* **532**, 1900491 (2020).

[61] R. Frésard and P. Wölfle, *Int. J. Phys. B* **6**, 685 (1992).

[62] V. H. Dao and R. Frésard, *Phys. Rev. B* **95**, 165127 (2017).

[63] W. Zimmermann, R. Frésard, and P. Wölfle, *Phys. Rev. B* **56**, 10097 (1997).

[64] R. Frésard and K. Doll, *Proceedings of the NATO ARW The Hubbard Model: Its Physics and Mathematical Physics*, eds. D. Baeriswyl, D. K. Campbell, J. M. P. Carmelo, F. Guinea, and E. Louis, San Sebastian (1993) (Plenum Press, 1995), p. 385.

[65] D. Riegler, M. Klett, T. Neupert, R. Thomale, and P. Wölfle, *Phys. Rev. B* **101**, 235137 (2020).

[66] V. V. Hovhannisyan, N. S. Ananikian, A. Campa, and S. Ruffo, *Phys. Rev. E* **96**, 062103.

[67] J.-P. Legré, G. Albinet, J.-L. Firpo, and A. M. S. Tremblay, *Phys. Rev. A* **30**, 2720 (1984).

[68] A. Bakchich, A. Benyoussef, and M. Touzani, *Physica A* **186**, 524 (1992).

[69] F. Antenucci, A. Crisanti, and L. Leuzzi, *Phys. Rev. E* **90**, 012112 (2014).

[70] A. Erdinç, O. Canko, and E. Albayrak, *J. Magn. Magn. Mater. A* **303**, 185 (2006).

[71] M. Tanaka and T. Kawabe *J. Phys. Soc. Jpn.* **54**, 2194 (1985).

[72] I. Dani, N. Tahiri, H. Ez-Zahraouy, A. Benyoussef, *Physica A* **407**, 295 (2014).

Appendix A: Further slave boson properties

The generic slave boson rewriting of the physical electron creation operators in terms of auxiliary particles Eq. (4) makes it manifest that any slave boson representation possesses an internal gauge symmetry group [47–49, 56–60]. In the present case of the two-band model and using the above four-valued spin-band index α the representation of the physical electron operators Eq. (4) is invariant under the gauge transformations

$$\begin{cases} f_{\alpha} \longrightarrow e^{-i\chi_{\alpha}} f_{\alpha} \\ e \longrightarrow e^{i\theta} e \\ p_{\alpha} \longrightarrow e^{i(\chi_{\alpha} + \theta)} p_{\alpha} \\ d_{\alpha, \alpha'} \longrightarrow e^{i(\chi_{\alpha} + \chi_{\alpha'} + \theta)} d_{\alpha, \alpha'} \\ t_{\alpha, \alpha', \alpha''} \longrightarrow e^{i(\chi_{\alpha} + \chi_{\alpha'} + \chi_{\alpha''} + \theta)} t_{\alpha, \alpha', \alpha''} \\ \varpi \longrightarrow e^{i(\theta + \sum_{\alpha} \chi_{\alpha})} \varpi \end{cases} \quad (\text{A1})$$

The gauge symmetry group is therefore $U(1) \times U(1) \times U(1) \times U(1) \times U(1)$. The Lagrangian also possesses this symmetry. Expressing the bosonic fields in amplitude and phase variables as

$$\begin{aligned} e(\tau) &= \sqrt{R_e(\tau)} e^{i\theta(\tau)} \\ p_{\alpha}(\tau) &= \sqrt{R_{\alpha}(\tau)} e^{i(\chi_{\alpha}(\tau) + \theta(\tau))} \end{aligned} \quad (\text{A2})$$

allows to gauge away the phases of the above five slave boson fields, provided one introduces the five time-dependent Lagrange multipliers

$$\begin{aligned} \lambda'(\tau) &\equiv \lambda' + \partial_{\tau} \theta(\tau) \\ \lambda_{\alpha}(\tau) &\equiv \lambda_{\alpha} - \partial_{\tau} \chi_{\alpha}(\tau). \end{aligned} \quad (\text{A3})$$

Here the radial slave boson fields are implemented in the continuum limit [56–58], but introducing radial slave boson fields can also be achieved in the discrete time step set-up [48, 49, 60].

As these bosonic fields have been deprived of their phase degree of freedom they do not undergo Bose condensation any longer. In fact, their exact expectation values are generically non-vanishing [49] (see Ref. [48] in the case of Barnes' representation to the single impurity Anderson model), and may be approximately obtained through the saddle-point approximation (SPA) that we used above. This approximation is exact in the large degeneracy limit, with Gaussian fluctuations generating the $1/N$ corrections [61] (for a recent detailed reference, see Ref. [62]). It has been tested against quantum Monte Carlo simulations in the most challenging $N = 2$ case: A quantitative agreement for charge structure factors was

demonstrated [63] and, for example, a very good agreement on the location of the metal-to-insulator transition for the honeycomb lattice has been shown [64]. Also the comparison of ground state energies to numerical simulations are excellent [39]. Further quantitative agreement of ground state energies and site-dependent local magnetization with density matrix embedded theory have been recently reported [65].

We now turn to the operator $z_{i,\alpha}$. It represents the change in the bosonic occupations which results from the annihilation of an electron (see of Eq. (4)). In the considered paramagnetic phase one introduces z through $z \equiv z_{i,\alpha}$. Following Ref. [11] it reads:

$$z = L\tilde{z}R \quad (\text{A4})$$

with

$$\tilde{z} = ep + (p+t)(d_P + d_A + d_H) + t\varpi \quad (\text{A5a})$$

$$L = (1 - p^2 - d_P^2 - d_A^2 - d_H^2 - 3t^2 - \varpi^2)^{-\frac{1}{2}} = (1 - n_\alpha)^{-\frac{1}{2}} \quad (\text{A5b})$$

$$R = (1 - e^2 - 3p^2 - d_P^2 - d_A^2 - d_H^2 - t^2)^{-\frac{1}{2}} = n_\alpha^{-\frac{1}{2}} \quad (\text{A5c})$$

and $n_\alpha \equiv \frac{n}{4}$. Note that z depends on the three d -fields in a symmetric fashion.

Appendix B: Saddle-point equations

The saddle-point equations associated to the derivative with respect to the bosons read:

$$\lambda' + \left[p + \frac{\tilde{z}e}{n_\alpha}\right] \frac{2\mathcal{B}}{e} = 0 \quad (\text{B1})$$

$$\lambda' - \lambda + \left[e + d_P + d_A + d_H + \tilde{z}p \frac{3 - 2n_\alpha}{n_\alpha(1 - n_\alpha)}\right] \frac{\mathcal{B}}{2p} = 0 \quad (\text{B2})$$

$$\lambda' - 2\lambda + U_P + \left[p + t + \frac{\tilde{z}d_P}{n_\alpha(1 - n_\alpha)}\right] \frac{\mathcal{B}}{d_P} = 0 \quad (\text{B3})$$

$$\lambda' - 2\lambda + U_A + \left[p + t + \frac{\tilde{z}d_A}{n_\alpha(1 - n_\alpha)}\right] \frac{\mathcal{B}}{d_A} = 0 \quad (\text{B4})$$

$$\lambda' - 2\lambda + U_H + \left[p + t + \frac{\tilde{z}d_H}{n_\alpha(1 - n_\alpha)}\right] \frac{\mathcal{B}}{d_H} = 0 \quad (\text{B5})$$

$$\lambda' - 3\lambda + U_P + U_A + U_H + \left[\varpi + d_P + d_A + d_H + \frac{\tilde{z}t(1 + 2n_\alpha)}{n_\alpha(1 - n_\alpha)}\right] \frac{\mathcal{B}}{2t} = 0 \quad (\text{B6})$$

$$\lambda' - 4\lambda + 2(U_P + U_A + U_H) + \left[t + \frac{\tilde{z}\varpi}{(1 - n_\alpha)}\right] \frac{2\mathcal{B}}{\varpi} = 0 \quad (\text{B7})$$

where we introduced

$$\begin{aligned} \bar{\epsilon} &\equiv \sum_{\mathbf{k},\nu} f_F(E_{\mathbf{k},\nu}) \epsilon_{\mathbf{k},\nu}^{(0)} \\ \mathcal{B} &\equiv \frac{\tilde{z}\bar{\epsilon}}{n_\alpha(1 - n_\alpha)}. \end{aligned} \quad (\text{B8})$$

Here, $f_F(\dots)$ is the Fermi function. Steps towards the solution of the saddle-point equations involve solving

Eqs. (B1, B7) with respect to λ and λ' . One finds:

$$\begin{aligned} \lambda &= \frac{U_P + U_A + U_H}{2} + \left(\frac{t}{\varpi} - \frac{p}{e} + \frac{\tilde{z}(2n_\alpha - 1)}{n_\alpha(1 - n_\alpha)}\right) \frac{\mathcal{B}}{2} \\ \lambda' &= -2\left(\frac{p}{e} + \frac{\tilde{z}}{n_\alpha}\right) \mathcal{B} \end{aligned} \quad (\text{B9})$$

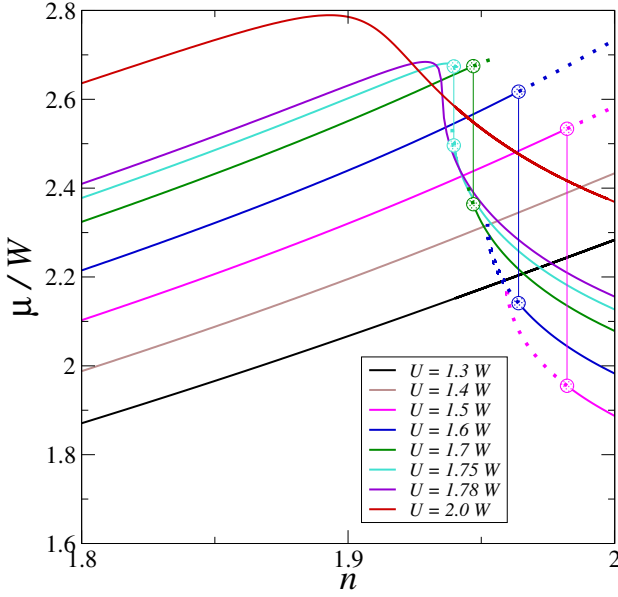


FIG. 14. Chemical potential in dependence on filling n for $J_H = W/6$. The circles and the vertical thin lines mark the first order transitions. The dotted curves refer to metastable states.

Inserting these solutions into Eqs. (B3, B4, B5) allows to write :

$$\begin{aligned}
 U_H - U_P &= \left(\frac{1}{d_P} - \frac{1}{d_H} \right) (p+t)\mathcal{B} \\
 U_A - U_P &= \left(\frac{1}{d_P} - \frac{1}{d_A} \right) (p+t)\mathcal{B} \\
 U_H - U_A &= \left(\frac{1}{d_A} - \frac{1}{d_H} \right) (p+t)\mathcal{B}. \quad (\text{B10})
 \end{aligned}$$

A useful relation between the three d -bosons may be derived out of these equations:

$$d_H = \frac{d_P d_A}{3d_P - 2d_A} \quad (\text{B11})$$

which both eases the numerical task and the interpretation of the results. Further steps towards the solution of the saddle-point equations arise from the derivatives with respect to the Lagrange multipliers. They read:

$$e^2 + 4p^2 + 2(d_P^2 + d_A^2 + d_H^2) + 4t^2 + \varpi^2 - 1 = 0 \quad (\text{B12})$$

$$4p^2 + 4(d_P^2 + d_A^2 + d_H^2) + 12t^2 + 4\varpi^2 - n = 0 \quad (\text{B13})$$

They may be solved with respect to e and ϖ as:

$$e^2 = 1 - n_\alpha - (3p^2 + d_P^2 + d_A^2 + d_H^2 + t^2) \quad (\text{B14})$$

$$\varpi^2 = n_\alpha - (p^2 + d_P^2 + d_A^2 + d_H^2 + 3t^2). \quad (\text{B15})$$

Altogether, one is left with four unknowns (p , d_P , d_A , and t) determined by Eqs. (B2, B3, B4, B6) rewritten using Eqs. (B9, B14, B15).

Appendix C: Chemical potential

A key quantity that reveals the addressed first order transition is the chemical potential which is depicted in Fig. 14. For $U < U_{\text{MI}} \simeq 1.41 W$ and starting from a large hole doping value, it is found that the chemical potential monotonically grows with increasing density, which ensures positive electronic compressibility and thermodynamical stability of this coherent metallic phase, as indicated by its quasiparticle residue $z^2 > 0.5$. Furthermore μ monotonically increases with U . However, if U exceeds U_{MI} , a bad metal state stabilizes close to half filling and μ jumps to a lower value and decreases further towards half filling.

If U exceeds U_{CEP} the chemical potential first grows but then reaches a maximum and decreases until the metallic solution ceases to exist. Accordingly, the density dependence of μ reveals a charge instability—signaled by the resulting negative electronic compressibility. This metallic, negative compressibility state is superseded in a first order transition to a bad metal state when n is further increased.

Above U_c^* the continuity of the density dependence of the chemical potential is restored. Though continuous, these curves are characterized by a maximum which implies that the charge instability persists above U_c^* . The latter is a hallmark of the doped Mott insulator.

Appendix D: Single and triple occupancies

In a fashion similar to the d -bosons the critical end point (U_c^*, n^*) is also central to the density dependence of the p and t bosons; there, they both exhibit an inflection point with diverging derivative with respect to n . For $U > U_c^*$ inflection points remain, though less visible, while the amplitude of the derivatives diminishes when moving away from the critical point. For $U < U_c^*$ all bosons jump at the first order transition, and a smooth behavior is restored for $U < U_c(2)$. Similar comments apply to the bosons p and t involving single and triple occupancy, respectively: as shown in Figs. 15(a) and (b) they vanish in the Mott insulating phase, and exhibit related inflection points at the critical end point (U_c^*, n^*). It should also be noticed that t increases when slightly hole-doping the Mott insulator ($\delta \lesssim 10\%$). This leads to a sizeable gain of kinetic energy for electrons moving in a background of essentially doubly occupied sites and reinforces the coherence of the quasiparticles that is lost in the Mott insulating phase.

Appendix E: BEG-parameters

In Section IV we have set up the BEG scheme as a phenomenological approach to model the bosonic degrees of freedom. In principal, one can devise a microscopic approach through a strong coupling expansion or Schrieffer-

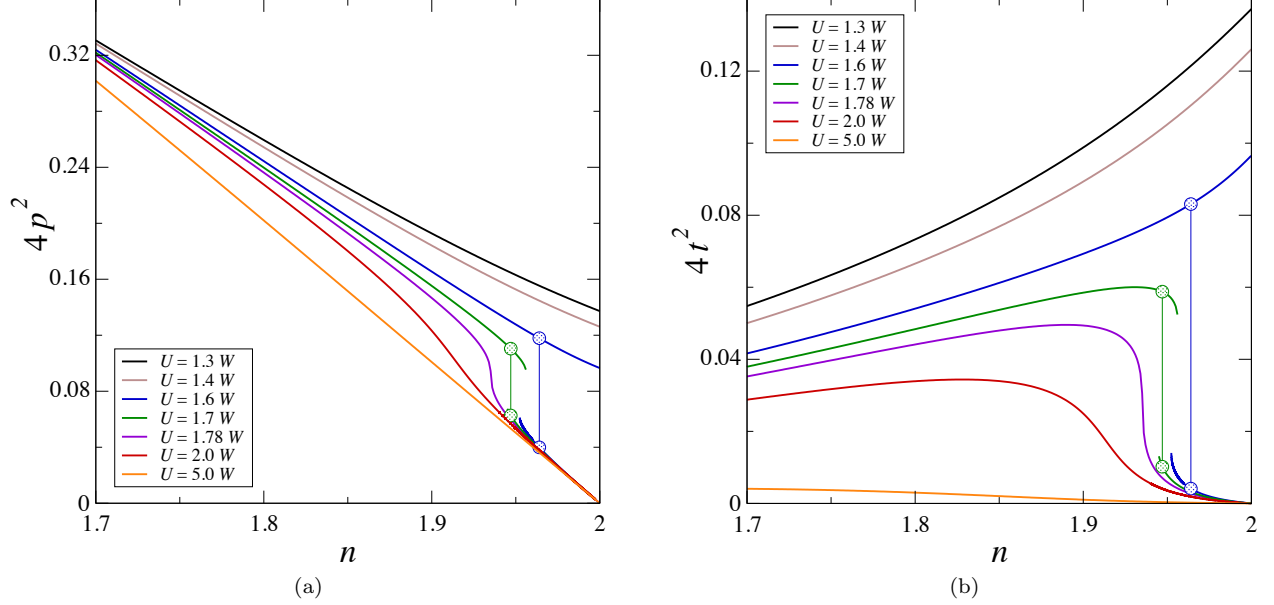


FIG. 15. Single (a) and triple (b) occupancy in dependence on filling n for $J_H = W/6$. The circles and the vertical thin lines characterize the first order transitions.

Wolff transformation in order to project onto a subspace with no triple and quadruple occupied sites. Such an expansion generates nearest-neighbor exchange terms. If it is assumed that only configurations with d_P and d_A are relevant, then the Hamiltonian contribution for double occupancies reads

$$\begin{aligned}
 \mathcal{H}_{P,A} = & (U - 3J_H) \sum_{i=1}^{N_L} n_{P_i} + (U - 2J_H) \sum_{i=1}^{N_L} n_{A_i} \\
 & - V_{PA} \sum_{\langle i,j \rangle} (n_{P_i} n_{A_j} + n_{A_i} n_{P_j}) \\
 & - V_{PP} \sum_{\langle i,j \rangle} n_{P_i} n_{P_j} - V_{AA} \sum_{\langle i,j \rangle} n_{A_i} n_{A_j} \\
 & - \mu \sum_{i=1}^{N_L} (n_{P_i} + n_{A_i}) - \mu N_L \quad (\text{E1})
 \end{aligned}$$

where n_{P_i} (n_{A_i}) is the number operator for a d_P - (d_A)-configuration on site i . In the expression with the chemical potential one expects $-\mu \sum_{i=1}^{N_L} (n_{p_i} + 2n_{P_i} + 2n_{A_i})$ where n_{p_i} denotes the number operator for singly occupied sites and factors of two take into account that double occupied sites contribute two electrons. Yet, with the relation $\sum_{i=1}^{N_L} n_{p_i} = N_L - \sum_{i=1}^{N_L} (n_{P_i} + n_{A_i})$ one confirms the last line of Eq. (E1).

In Sec. IV we included the d_H -configurations through the constraint Eq. (B11) however those sites are not represented by a proper term in the Hamiltonian. This approach is justified if the number of such sites, that is d_H^2 , is much smaller than d_P^2 , d_A^2 and doping δ which is true close to the considered transition (compare Fig. 5(a), (b), (c), and Fig. 11). If one introduces the on-site en-

ergy $U \sum_{i=1}^{N_L} n_{H_i}$ for the sites with d_H -configuration then one can identify a shift of Δ , a quantity which is determined below, however this does not affect our results in a qualitative way.

Here we do not intend to determine the exchange coupling parameters V_{PP} , V_{AA} , and V_{PA} as functions of U , J_H , and t and t' explicitly. We rather discuss qualitatively their dependencies and use them as phenomenological parameters. It is our intention to gain an approximate understanding of the phase transitions identified

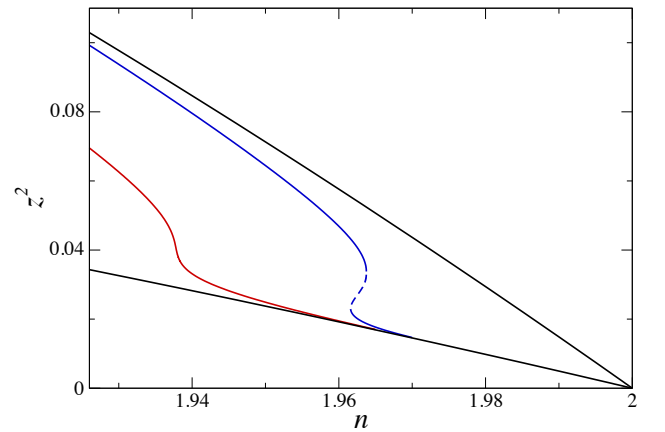


FIG. 16. Quasiparticle residue from BEG evaluation for finite \mathcal{L} . The black lines are the upper and lower bounds for z^2 from Eq. (22). Parameters are $\mathcal{J} = 0.0$, $\mathcal{L} = -1.0$, and $g_B = 20$ (red) for the continuous transition, and $\mathcal{J} = 0.1$, $\mathcal{L} = -0.9$, and $g_B = 180$ (blue) for the discontinuous transition. All energies are in units of $J_H/2$ and $h = 1.0$.

in slave boson theory within a much simpler framework. For this purpose we now relate the states of Hamiltonian (E1) to those of the generalized BEG-model (15) through the identification of $S_i = 1$ with the spin-parallel occupation of the two orbitals n_{P_i} , the pseudospin $S_i = -1$ with the spin-antiparallel occupation of the two orbitals n_{A_i} , and $S_i = 0$ with the single occupation n_{P_i} . This comparison of matrix elements of Hamiltonians (E1) and (15) yields the following relations:

$$\begin{aligned} h &= J_H/2, & \Delta &= U - \frac{5}{2}J_H - \mu \\ \mathcal{L} &= \frac{1}{4}(V_{PP} - V_{AA}), & \mathcal{K} &= \frac{1}{4}(V_{PP} + V_{AA} + 2V_{PA}) \\ \mathcal{J} &= \frac{1}{4}(V_{PP} + V_{AA} - 2V_{PA}) \end{aligned} \quad (\text{E2})$$

Obviously, the magnetic field h of the pseudospin is set by Hund's coupling J_H and the chemical potential related to the pseudospin particles, $-\Delta$, is determined by the chemical potential μ . However, we do not calculate Δ through μ directly but we gain Δ from the mean-field equation (25).

All exchange coupling parameters $V_{PP/AA/PA}$ are expected to be positive and of order $2t^2/U$ in the strong coupling regime where not only t but also J_H is sizably smaller than U ; we also take $(t'/t)^2 \ll 1$.

It is then reasonable to assume that \mathcal{L} and \mathcal{J} are considerably smaller than \mathcal{K} because terms of order t^2/U cancel in \mathcal{L} and \mathcal{J} on account of the minus signs in their respective relations (E2). The coupling \mathcal{L} is expected to be negative on account of $V_{PP} < V_{AA}$ which results from equal energies of excited states in both, $d_P - d_P$ and $d_A - d_A$, and lower energy in the ground state of the $d_P - d_P$ configuration (so the denominator in the strong coupling expression of the exchange energy is larger for $d_P - d_P$ than for $d_A - d_A$). Therefore we conclude that \mathcal{L} is negative, \mathcal{J} can have both signs, and \mathcal{K} is positive and much larger than the absolute value of either \mathcal{J} or \mathcal{L} .

In Sec. IV B we chose $\mathcal{L} = 0.0$. In Fig. 16 we show that a finite negative \mathcal{L} can produce similar results if the further parameters are chosen properly. In fact, a negative \mathcal{L} has a similar effect on the orbital magnetization m as a negative \mathcal{J} if q is close to 1.

Appendix F: BEG-phase-diagram

In Section IV we considered an antiferromagnetic version of the BEG-model as it allowed to address both, continuous and discontinuous transitions. The question then arises if the system is actually in an antiferromagnetic state or if the parameter regime is such that the state is still paramagnetic which we have assumed in our evaluation.

The phase diagram of the spin-1 BEG model was studied by mean field evaluations (see, for example, Refs. [53, 54, 66]), in renormalization-group analyses [67–69], with

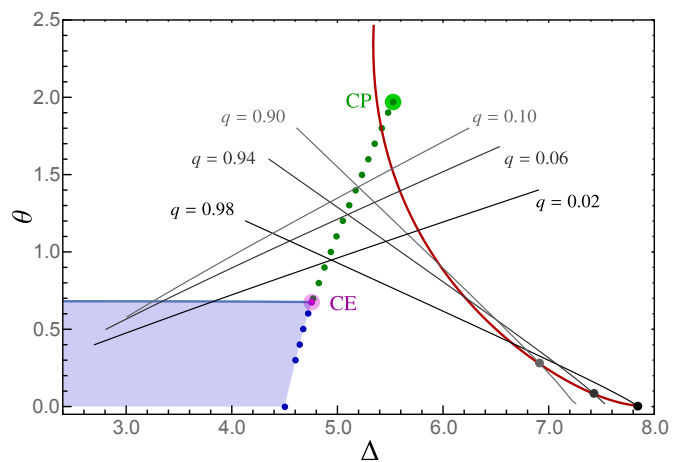


FIG. 17. BEG phase diagram. The parameters are $\mathcal{J} = -1.0$, $\mathcal{L} = 0.0$, and $\mathcal{K} = 8.0$; these energy parameters as well as temperature θ and chemical potential Δ of the pseudospins are in units of the field h . The blue line is the continuous phase transition from the antiferromagnetic state at low θ (blue area) to the paramagnetic state at high θ . The blue dots represent a first order transition line from the antiferromagnetic state to a paramagnetic state with lower values of q , and the green dots depict the first order transition line in the paramagnetic state, also from a higher to a lower value of q . CP is a critical point and CE is the critical end point. The gray curves connect states with fixed q -values. The red line is the curve in the parameter space (Δ, θ) for $g_{\text{FB}} = 50$ along which we move when we go from large doping ($n = 1.8$, that is $q = 0.70$ at the upper end point) to small doping ($n = 1.98$, that is $q = 0.98$ at the lower end point). For this curve θ is the effective temperature $k_B T_{\text{eff}}$. The black dots on that curve are placed at the actual crossing points with the lines of fixed q .

exact recursion relations on the Bethe lattice [70], and Monte Carlo techniques (see, e.g., Ref. [71, 72]), not the least because it reveals a plethora of phase transitions including a tricritical point in a certain parameter range.

In Fig. 17 the phase diagram is displayed for a set of parameters which we used in Section IV. A tricritical point is absent for this large value of \mathcal{K} . When Eq. (27) is solved for m at given q and the resulting $m(q)$ is inserted in Eq. (25), one can identify a curve $T_{\text{eff}}(\Delta)$ parameterized by q . This is the red curve in Fig. 17 where $k_B T_{\text{eff}}$ is the temperature θ . We also plot lines along which q is constant. It is only the lower crossing point of the constant- q lines with the $T_{\text{eff}}(\Delta)$ -curve that represents a solution of Eqs. (27) and (25).

Note that the slope of the constant- q lines changes sign when going from q close 1 to small values of q . At the first order transition (green dots) the high- q lines cross with appropriate low q -lines as there the q -value jumps when the thermodynamic equilibrium is considered (for example, a jump from $q = 0.98$ to approximately $q = 0.02$). In fact, high values of q represent the thermodynamic equilibrium on the left hand side of the transition (that is, for lower Δ) and low values of q are in equilibrium on

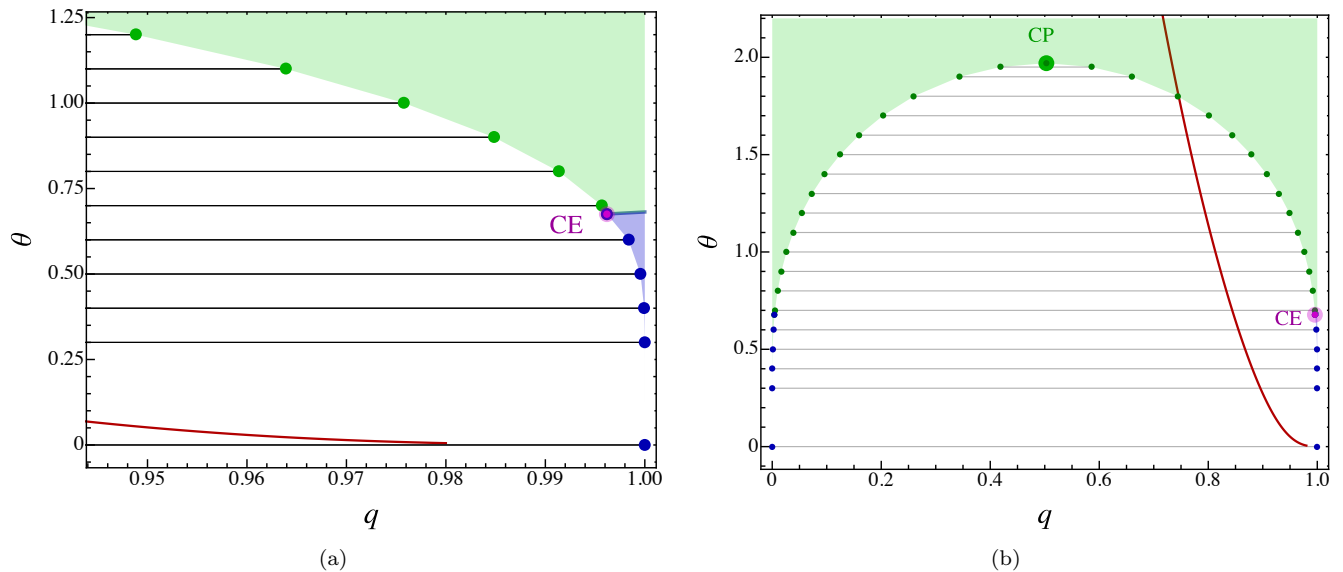


FIG. 18. BEG phase diagram in dependence on q . The parameters are $\mathcal{J} = -1.0$, $\mathcal{L} = 0.0$, and $\mathcal{K} = 8.0$; these energy parameters as well as the temperature θ of the pseudospins are in units of h . The blue triangular area represents the antiferromagnetic state (see panel (a)). The blue line depicts the continuous transition, the blue dots the first order transition from the antiferromagnetic state to a paramagnetic state, and the green dots refer to the first order transition in the paramagnetic state. The gray lines between these dots connect the equilibrium states with high q to those with low q at the first order phase transition (see panel (b)). States within the white area are not characterized by a global minimum of the BEG free energy. The green area is the regime where global minima of the free energy exist. CP is a critical point and CE is the critical end point. The red curve is given by $k_B T_{\text{eff}}(q)$ for $g_{\text{fb}} = 50$.

the right hand side of the transition (that is, for larger Δ).

From these considerations it is obvious that the states that we find as solutions from the mean-field equations are not equilibrium states of the pseudospin system: above approximately $q = 0.75$ (for $g_{\text{fb}} = 50$) the red curve is in the parameter regime where low values of q would be (global) equilibrium solutions whereas we are forced to realize high- q solutions because the filling n , which is approximately $1 + q$, approaches half-filling at $q = 1$ and the effective temperatures goes to zero.

The choice of the parameter space (Δ, θ) yields the

conventional representation of the phase diagram of the BEG model but here it appears to be more appropriate to consider functions of q instead of Δ on account of the necessity to specify the filling. Correspondingly we display in Fig. 18 the phase diagram in the parameter space (q, θ) . It can be clearly seen that the $k_B T_{\text{eff}}(q)$ -curve is placed in the nonequilibrium regime (white area) except for high temperature and q below 0.75 (green area). The antiferromagnetic regime (blue area) appears as a small triangle in this parameter space and it is well separated from the states that are relevant for the analysis of the phase transitions discussed in the present framework.